

The Mountain Front Flexure in the Lurestan region of the Zagros belt: Crustal architecture and role of structural inheritances

Tavani Stefano^{a,*}, Camanni Giovanni^a, Nappo Michele^a, Snidero Marco^a, Ascione Alessandra^a, Valente Ettore^a, Gharabeigi Gholamreza^b, Morsalnejad Davoud^b, Mazzoli Stefano^c

^a DISTAR, Università degli Studi di Napoli Federico II, Naples, Italy

^b N.I.O.C., Tehran, Iran

^c School of Science and Technology, Geology Division, University of Camerino, Italy

ARTICLE INFO

Keywords

Zagros
Inversion tectonics
Mountain front flexure
Balanced cross section

ABSTRACT

The Mountain Front Flexure is a major structure of the Zagros orogenic system, and is underlain by the deeply rooted and seismically active Mountain Front Fault system. These coupled structural features divide the belt from its foreland and their trace is sinuous, forming salients and recesses. The origin and tectonic significance of the Mountain Front Fault system and its sinuosity are still unclear, with most of hypotheses pointing to a strong structural control exerted by geological inheritances. In this work we combine interpretation of seismic reflection profiles, earthquake data, geomorphic analysis, and geological observations, to build a balanced cross section across the Mountain Front Flexure in the Lurestan region. Our data are suggestive of a hybrid tectonic style for the Lurestan region, characterised by a major and newly developed crustal ramp in the frontal portion of the belt (i.e the Mountain Front Fault) and by the reactivation of steeply dipping pre-existing basin-bounding faults, along with a minor amount of shortening, in the inner area. Specifically, the integration of our results with previous knowledge indicates that the Mountain Front Fault system developed in the necking domain of the Jurassic rift system, ahead of an array of inverted Jurassic extensional faults, in a structural fashion which resembles that of a crustal-scale footwall shortcut. Within this structural context, the sinusoidal shape of the Mountain Front Flexure in the Lurestan area arises from the re-use of the original segmentation of the inverted Jurassic rift system.

1. Introduction

The Mountain Front Flexure (MFF) is a major structure of the Zagros folded belt, consisting of a topographic and structural step that divides the belt from its foreland basin (Falcon, 1961). The MFF runs for more than 1000 km, from Kurdistan to Fars, to eventually disappear further to the SE, and is the surface expression of the active and deeply rooted Mountain Front Fault system (Fig. 1a). The trend of the Mountain Front Flexure is characterised by a sinusoidal shape defined by salients and recesses. From NW to SE these sinuosities are: the Kirkuk embayment, the Lurestan arc, the Dezful embayment, and the Fars arc (Fig. 1a). The Mountain Front Fault system which underlie the MFF comprises a seismically active basement-involving reverse fault system (e.g. Berberian, 1995; Talebian and Jackson, 2004; Sherkati and Letouzey, 2004; Molinaro et al., 2005; Mouthereau et al., 2006; Alavi, 2007; Vergés et al., 2011a; Tavani et al., 2018a), and the structural step across it is more than 3 km in the Kirkuk and Dezful em-

bayments and in the Lurestan arc, and less than 2 km in the Fars area (e.g. Sherkati et al., 2006; Emami et al., 2010).

Although there is a general consensus in the literature on that the sinusoidal shape of the Mountain Front Flexure and the Mountain Front Fault system is controlled by geological inheritances, their exact nature is controversial and the origin of the flexure is still uncertain. For example, McQuarrie (2004) has suggested that the position of the Mountain Front Flexure could be related to thickness variations of the Cambrian Hormuz salt, which is placed at the base of the sedimentary pile. Reactivation of steeply dipping N-S and E-W striking inherited basement faults, oriented obliquely to the NE-SW shortening direction, has been instead proposed by several authors (e.g. Hessami et al., 2001; Sepehr and Cosgrove, 2004; Lawa et al., 2013), in accordance with the documented occurrence of inherited N-S and E-W striking faults exposed in the Arabian plate (e.g. Talbot and Alavi, 1996; Hessami et al., 2001). The Mw 7.3 Ezgeleh earthquake, that hit the Lurestan region on November 12, 2017, along with its aftershocks have illuminated the geometry at depth of one of the N-S striking

* Corresponding author. Dipartimento di Scienze della Terra, dell'Ambiente e delle Risorse. Università degli Studi di Napoli Federico II, Via Cupa Nuova Cintia, 21, 80126, Naples, Italy.
E-mail address: stefano.tavani@unina.it (T. Stefano)

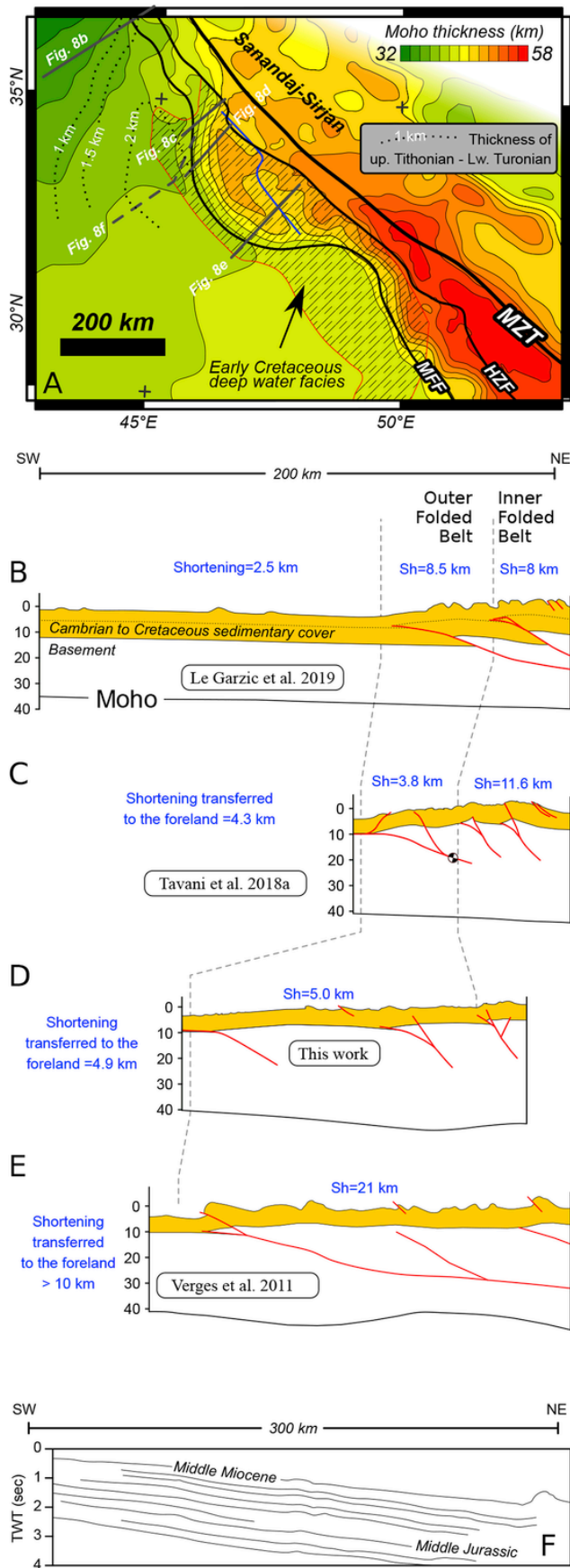


Fig. 1. Tectonic sketch map of the Zagros Mts. (A) Elevation map with major structural features indicated. (B) Elevation map (source: ESDIS) showing the main structures of the NW portion of the Lurestan arc, with the Ezgeleh Mw 7.3 seismic sequence indicated (source: USGS, <https://earthquake.usgs.gov>).

oblique portions of the Mountain Front Fault system (Fig. 1b), which was revealed to consist of a low-dipping N-S striking oblique ramp, placed at about 20 km depth within the basement (e.g. Chen et al., 2018; Tavani et al., 2018a; Gombert et al., 2019; Vajedian et al., 2018). The low dip of this structure is suggestive of a model in which the Mountain Front Fault system is comprised of, at least in the Lurestan arc, newly-formed shallowly-dipping frontal (Blanc et al., 2003; Vergés et al., 2011a; Le Garzic et al., 2019) and oblique ramps (Tavani et al., 2018a). This apparently contrasts with the idea that the sinusoidal shape of the Mountain Front Fault system can be controlled by the reactivation of steeply dipping pre-existing basement faults or at least requires that steeply dipping faults are connected with shallow dipping faults at depth.

In this work, we explore the geometric complexities of the Mountain Front Fault system in the Lurestan arc, by integrating seismic reflection sections interpretation, cross section balancing, geomorphic analysis, and data from the aftershock sequence of the 2017 Ezgeleh Mw 7.3 earthquake. Limited shortening at the higher structural levels of the belt, where no remarkable far-travelled thrusts occur, allow to place constraints on the nature of the faults underlying the major topographic and basement steps of the area. Nodal planes of large earthquakes (Mw > 5) placed at short distances from the studied section constrain the Mountain Front Fault system at depth. Our results demonstrate that: (i) the low amount of shortening requires an inversion tectonic style along most portions of the studied section; (ii) the Mountain Front Fault system is comprised of a shallowly-dipping mid-crustal ramp splaying off the foot-wall of an inverting basement fault system; (iii) the Mountain Front Flexure is, in essence, the frontal limb of a slightly transported fault-propagation fold developing above the tip of the Mountain Front Fault system; (iv) the distribution of pre-existing faults is a primary factor in controlling the development and the shape of the frontal structural features of the Zagros belt in the Lurestan area.

2. Geological setting

The Zagros belt extends from Turkey to SE Iran (Fig. 1a), and developed in Late Cretaceous to Cenozoic time. Convergence started with the closure of the Neo-Tethys ocean and evolved, during the late Eocene-Oligocene, in the continental collision between the Eurasian and Arabian plates (e.g. Stöcklin, 1968; Ricou et al., 1977; Berberian and King, 1981; Dercourt et al., 1986; Braud, 1987; Alavi, 1991, 1994; Stampfli and Borel, 2002; Agard et al., 2005; Allen and Armstrong, 2008; McQuarrie and van Hinsbergen, 2013; Koshnaw et al., 2018). The Zagros belt develops on the Arabian plate and it is bounded to the NE by the Main Recent Fault and the Main Zagros Thrust that represent the NW-SE trending suture zone that separates the Arabian plate from the Sanandaj-Sirjan Zone on the Eurasia plate to the NE (Fig. 1a) (e.g. Berberian and King, 1981; Ziegler, 2001; Blanc et al., 2003; Ghasemi and Talbot, 2006). The collisional zone is currently accommodating oblique convergence, with the 2 cm/yr N-ward motion of Arabia (considering fixed the Eurasia plate; Vernant et al., 2004) being partitioned between right-lateral motion along the NW-SE-striking suture zone and NE-SW-oriented shortening within the Zagros belt (Blanc et al., 2003; Vernant et al., 2004; Talebian and Jackson, 2002, 2004). In detail, shortening in the Zagros belt is about 5–10 mm/yr (Vernant et al., 2004), and it is accommodated by NW-SE oriented thrust and folds.

Until the Cretaceous and before the closure of the Neo-Tethys, the Zagros Belt and the Sanandaj-Sirjan Zone formed the two conjugate passive margins of a southern branch of the Neo-Tethys (Berber-

ian and King, 1981; Blanc et al., 2003; Sepehr and Cosgrove, 2004; Vergés et al., 2011a; Wrobel-Daveau et al., 2010). The Zagros belt is made up of terrains that originally belonged to the SW passive margin of the Neo-Tethys (NE Gondwana), i.e. the Arabian continental margin (Ziegler, 2001; Sepehr and Cosgrove, 2004; Ghasemi and Talbot, 2006; Vergés et al., 2011a; Mouthereau et al., 2006, 2012; English et al., 2015; Tavani et al., 2018b). This passive margin was characterised by different extensional domains. In particular, the distal portion of the margin included a deep-water radiolarite basin (Kermanshah Radiolarite basin), and an isolated carbonate platform (Bisotun Platform) interposed between the radiolarite basin and the oceanic domain (e.g. Ricou et al., 1977; Braud, 1987; Wrobel-Daveau et al., 2010). These extensional domains developed during the Permo-Triassic (e.g. Alavi, 1980; Berberian and King, 1981; Ghasemi and Talbot, 2006) and, mostly, Early Jurassic (e.g. Tavani et al., 2018b) rifting events, which lead to the divergence of the Arabian margin and the Sanandaj-Sirjan Zone, and to the opening of the above mentioned southern branch of the Neo-Tethys. The distal portion of the Arabian margin is presently exposed in the hanging wall of the High Zagros Fault (Fig. 1), a fault that has been active since the Late Cretaceous (Karim et al., 2011; Saura et al., 2015). The proximal domain of the Arabian margin is now cropping out in the footwall of the High Zagros Fault, which is the Simply Folded Belt, where NW-SE trending folds with up to 10 km wavelengths occur in a 200 km wide area, delimited to the SW by the Zagros Deformation Front (Fig. 1a).

The Mountain Front Flexure and the underlying Mountain Front Fault system, which are the object of investigation of this paper, are located between the NW-SE striking High Zagros Fault and the Zagros Deformation Front. In particular, the flexure represents a major topographic and structural divide that separates a north-eastern area, where thrust faults affect the basement, from a south-western area, mostly characterised by folds confined within the sedimentary sequence (or at least with no striking evidence of basement-involved reverse faults). In the Lurestan arc, one of the most prominent sinuosities of the mountain belt, the frontal features of the belt are characterised by a frontal portion striking NW-SE, and two lateral segments striking roughly E-W (SE segment, Bala Rud segment) and N-S (NW segment, Kanaquin segment), the latter being part of the study area of this work (Figs. 1b and 2). Fold traces are slightly bent approaching these oblique segments, but no remarkable offsets can be observed across them (e.g. Alavi, 2007; Allen and Talebian, 2011; Casciello et al., 2011; Casini et al., 2018). In the NW portion of the Lurestan arc, the folded belt in the footwall of the High Zagros Fault can be further divided into an outer and an inner folded belt (Fig. 1b), which are separated by a structural step marked by changes in elevation of nearly 2 km (Tavani et al., 2018a). In the study area, the High Zagros Fault is characterised by a major bend and by a more external position with respect to the NW. As a result, most of the inner folded belt is now located below the High Zagros Fault and our reconstruction is mostly limited to the outer folded belt (Fig. 2).

The sedimentary sequence of the Arabian margin exposed in the footwall of the High Zagros Fault, includes a pile of clastics and carbonates more than 10 km thick (James and Wynd, 1965; Stöcklin, 1968; Koop and Stoneley, 1982). In the south-eastern portion of the Zagros belt, i.e. in the Fars arc and in the Izeh domain (located immediately to the NE of the Dezful embayment), the base of the sedimentary sequence is represented by the late Proterozoic to early Cambrian Hormuz Salt, which does not occur in the Lurestan arc (e.g. Bahroudi and Koyi, 2003; Alavi, 2007). In detail, the sedimentary sequence of the Lurestan arc area starts with an about 3 km thick succession of Paleozoic continental clastic deposits (up to 6 km to the NW of the study area, in the Kurdistan region, according to Le Garzic et al., 2019), overlain by nearly 1 km of shallow-water carbonates of the Chia Zairi Formation, capped by the Triassic shales of the Bedu Shales and

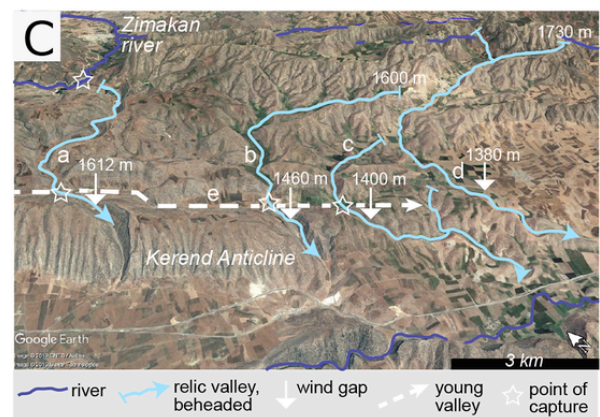
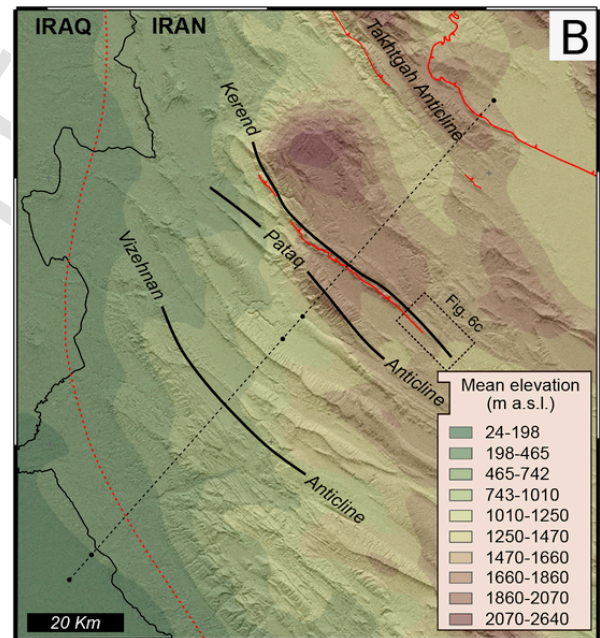
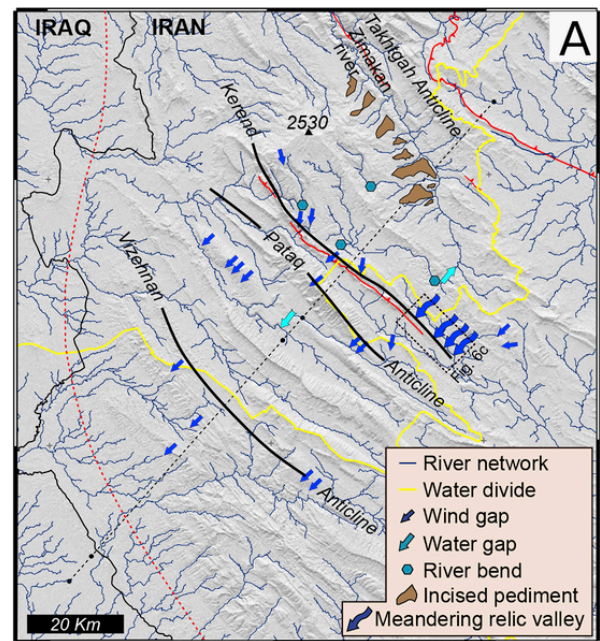


Fig. 2. Geological map of the study area along with: (i) density contour of remotely sensed and field measured bedding data; (ii) $M_w > 5$ earthquakes with moment tensor solution (2017–2019 time interval; source: USGS, <https://earthquake.usgs.gov>); (iii) traces of near-vertical seismic profiles and wells; (iv) a trace of the geological section in Figs. 4 and 7; (v) stratigraphic succession of the area. The inset shows the normalised frequency distribution of earthquakes depth occurred in the map area, with no time range restriction. Data are from the USGS and Iranian Seismological Centre (<http://irsc.ut.ac.ir>) catalogues.

Mirga Mir formations (Fig. 2) (Jassim and Goff, 2006; Bordenave, 2008). The overlying Triassic-Jurassic multilayer is exposed 50 km to the north of the study area and includes (Tavani et al., 2018b): the about 400 m thick Middle Triassic Geli Khana Formation, consisting of thin-bedded limestones and dolostones; the 600–700 m thick Late Triassic thick-bedded dolostones and limestones of the Kurra Chine Formation; the 30–100 m thick Late Triassic shales and thinly bedded dolostones of the Baluti Shale Formation; the 300 m thick dolostones of the Upper Triassic-Lower Jurassic Sarki and Sehkaniyan formations. The above described Permian to Early Jurassic stratigraphic succession was deposited in a shallow-water to continental environment. At the end of the Early Jurassic, a major subsidence pulse associated with a rifting event led to the drowning of the margin (Tavani et al., 2018b) and the onset of deep-water conditions and the deposition of nearly 100 m of deep-water limestones, marls, shales, and deep water evaporites (Sargelu, Naokelekan, and Barsarin formations, Toarcian to Tithonian), followed by 400–1000 m of Cretaceous basinal limestones, shales and marls (Garau, Sarvak and Ilam formations). To the SE of the study area, the upper portion of the Cretaceous sequence gradually passes from pelagic to neritic facies (Casciello et al., 2011). Further to the SW of the Mountain Front Flexure, the drowning of the carbonate platform was limited, and the Jurassic to Cretaceous stratigraphic succession was deposited mostly in a shallow marine environment (e.g. Ziegler, 2001). Onset of convergence during the Late Cretaceous caused the development of a first foredeep, filled by about 2 km of Maastrichtian to Eocene sediments (e.g. Homke et al., 2009; Vergés et al., 2011a; Saura et al., 2015). These are overlain by nearly 300–500 m of Oligocene-lower Miocene shallow-water carbonates (Shahbazan and Asmari formations), passing upward into lower to middle Miocene evaporites of the Gachsaran Formation. Renewed shortening affected this portion of the Zagros belt during Miocene (e.g. Barber et al., 2018) and led to the development of a second younger foredeep, filled by the Agha Jari and Bakhtiari clastic formations. The age of these formations in the study area has been determined by means of magnetostratigraphy, dating the base of the Agha Jari Formation at about 12–13 Ma and the base of the Bakhtiari at about 3 Ma (Homke et al., 2004). However, based on Sr strontium stratigraphy, a slightly older age (16 Ma) has been proposed for the lower part of the Agha Jari by Pirouz et al. (2015).

3. Data and methods

For determining the structure of the Mountain Front Flexure and of the underlying Mountain Front Fault system, we used a multidisciplinary methodological approach drawing from several independent datasets. These datasets include: seismic reflection profiles calibrated with borehole data, geological data, geomorphic data, and earthquake hypocenter and focal mechanism data. These datasets were analysed separately (see section 4) and, subsequently, combined together to construct the balanced cross section presented in section 5.

The seismic reflection profiles were acquired in different campaigns by the National Iranian Oil Company, in a time period spanning from the 2005 through to 2018. Twentyfive seismic reflection profiles (for a total length of about 1200 km) have been interpreted in this work for defining the deep geometry of faults and folds (Fig. 2). Nine and sixteen of the profiles are oriented, respectively, parallel (strike lines) and perpendicular (cross lines) to the traces of the folds that form the struc-

tural architecture of the belt. Although large portions of the study area are characterised by the occurrence of exposed karstified limestone (i.e. mostly the Asmari Formation), the seismic signal provide most sections with a resolution adequate for a reliable seismic interpretation. Furthermore, calibration of the seismic sections with surface geology data and the incorporation of seven wells (Fig. 2) which reached the Cenozoic (1 well), Cretaceous (1 well), Jurassic (3 wells), and Triassic (2 wells) units, provided further constraints for the firm interpretation of several portions of the study area.

Geological data comprise geological maps, and remotely sensed and field measured bedding dip data that were combined together to construct geological cross-sections across the study area. In particular, bedding dip data at a distance of < 2 km from the trace of the cross section have been projected onto it, and the geological cross section has been built by means of the 3DMove software package. To digitally extract traces of layers and transform them in bedding dip orientation, publicly available 0.5 m orthophotos draped onto 30 m resolution ASTER GDEM were used (e.g. Fernández, 2005; Snidero et al., 2011). This operation was performed by means of the OpenPlot software package (Tavani et al., 2011). Measured ($n: 337$) and remotely sensed ($n: 3499$) bedding surfaces are NW-SE striking (Fig. 2), consistently with the trend of the fold traces as shown in the geological map of the area (Fig. 2). Notably, remotely sensed data tend to overestimate gently dipping bedding (Fig. 2), as the digital extraction of traces needs non col-linear traces, which is hampered for steeply dipping strata.

The geomorphological analysis was based on the inspection of the large-scale features (30 m resolution DEM), both active and relic, associated with the topography and drainage network within the study area. This analysis was carried out by means of investigation of satellite images (Google Earth, 2019) and orthophotos, aided by a GIS-based analysis of digital topography data (30 m resolution ASTER GDEM). In particular, digital topography data were used to build a swath profile (generated by the SwathProfiler Add-in of Arcgis®; Pérez-Peña et al., 2017), a map showing the spatial distribution of elevation parameters, and to extract a digital stream network, which was validated through its comparison with a manually digitized drainage network constructed through the visual inspection of remotely sensed images. The satellite image inspection was also aimed at identifying relic stream paths and river bends. These features are of significant importance as they represent evidence of changes in flow orientations, which take place in response to local short-lived surface changes and/or regional long-term external processes driven by the differential influence of erosional or tectonic processes and, among the latter ones, fold growth (e.g. Keller et al., 1999; Lavé and Avouac, 2001; Miller and Slingerland, 2006; Ramsey et al., 2008; Prince et al., 2011; Walker et al., 2011; Obaid and Allen, 2017; Forte et al., 2015; Burberry et al., 2010; Bretis et al., 2011; Buscher et al., 2017).

Earthquake hypocentre and focal mechanism data were used to constrain the geometry of the fault systems at depth within the study area. These data are from the publicly available USGS earthquake catalogue (<https://earthquake.usgs.gov/earthquakes/search/>). In particular, in this study we selected seismic events with $M_w > 4$ occurred in the Lurestan region in a time period between november 12, 2017 and June 9, 2019, all of them (both reverse and strike-slip) being consistent with NE-SW oriented shortening. We chose this earthquake magnitude and this time frame, since the main aim here was to study earthquakes with a significantly high magnitude related to the $M_w 7.3$, November 12, 2017 earthquake that appeared to have activated a crustal shallowly-dipping fault within the study area of particular significance for this study. In addition, in the area of Fig. 2, we used the entire datasets in the catalogue of both the USGS and the Iranian Seismological Centre (<http://irsc.ut.ac.ir>) to determine the frequency of earthquake depth (inset in Fig. 2). This serves to place a rough limit between the brittle and ductile crust.

4. Results

4.1. Seismic reflection profiles

In this section, the interpretation of four representative seismic reflection sections is presented (Fig. 3): sections 1 and 2 are complementary and cross the whole study area largely overlapping with the trace of the balanced cross section (Fig. 2); sections 3 and 4 allow further constraining structures at the SW and NE edges of the balanced cross section, respectively. Where possible, up to five reliable (i.e. calibrated with borehole and/or surface geology data) stratigraphic horizons have been interpreted. From the youngest to the oldest, these stratigraphic horizons correspond to the Top Gachsaran (middle Miocene), the Top Asmari (lower Miocene), the Base Shahbazan (Oligocene), the Top Ilam (upper Cretaceous), and the Top Sehkaniyan (lower Jurassic) (Fig. 3). In addition, a reflector within the Triassic and three reflectors within the Paleozoic have been locally imaged, although they could have not been assigned to specific stratigraphic horizons. Finally, where possible, some intraformational horizons were also mapped to facilitate reconstructing geometries in specific areas.

Section 1 is characterised by a broad area in its central and NE parts that is affected by remarkable noise and poor resolution (Fig. 3). A few discontinuous reflectors can be traced in this area, although their stratigraphic attribution is harduous. In contrast, the southern part of the section shows a 20 km wide SW-dipping monocline, in which reflectors

tors of the Agha Jari, Gachsaran, and Asmari formations are nearly parallel to one another. More in detail, folds with wavelengths of 1–2 km affect the Asmari Formation and they are apparently sealed by the Gachsaran Formation (Fig. 3). This apparent growth stratal geometry is arising from the decoupling taking place along the Gachsaran evaporites, as already documented in the area (e.g. Fig. 14c in Vergés et al., 2011b).

Section 2 is less affected by noise, and reflectors can be more easily traced and correlated across the section. Particularly, the Paleozoic to Early Jurassic (i.e. Top Sehkaniyan) stratigraphic package is characterised by nearly parallel reflectors. Nevertheless, some thickness variations do exist between the Paleozoic 1 and Paleozoic 2 reflectors, which could be related with growth structures, previously described in the Zagros, developed during the Permo-Triassic rifting (e.g. Sepéhr and Cosgrove, 2004). However, besides these variations and the local folding occurring at the Pataq Anticline, the Paleozoic to Early Jurassic sequence forms a gently NE-dipping regional monocline which is particularly apparent in the SW portion of the section. This monocline is abruptly interrupted at the location of the Mileh Sorkh, Kerend, and Takhtgah anticlines. Moving upward in the stratigraphy, the Top Ilam reflector follows this general monoclinal trend although being not always parallel to the underlying Top Sehkaniyan reflector. This can be due to: (i) the partial decoupling between the Ilam and Sehkaniyan formations taking place at the Garau marls and shales, and which resulted in the development of diffuse disharmonic folding of the Ilam Formation (e.g. to the NE of the Kerend Anticline), and (ii) the occurrence

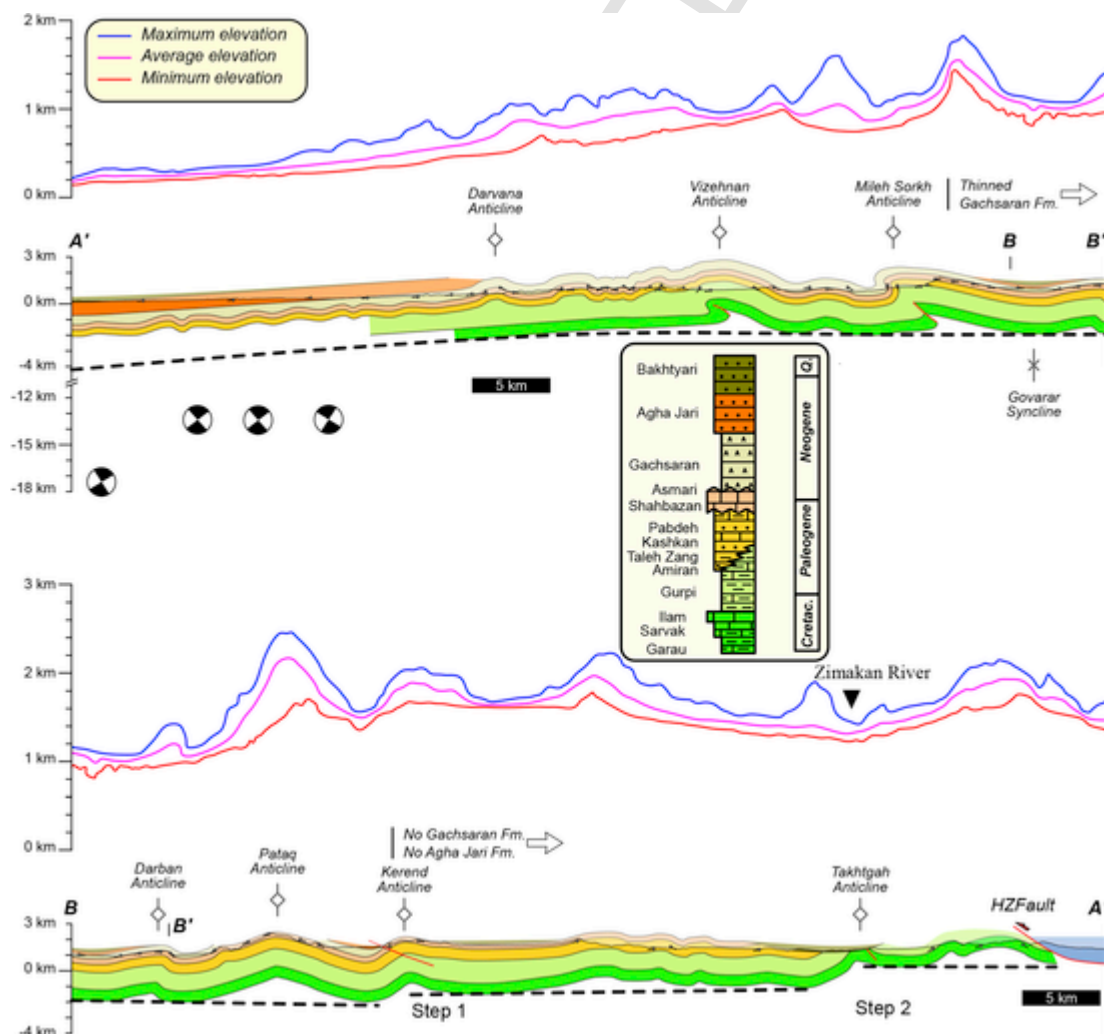


Fig. 3. NE-SW-oriented near-vertical seismic profiles with along with line drawing.

of Early Jurassic extensional troughs, filled by the Middle Jurassic to Cretaceous sediments (Tavani et al., 2018b). Similar disharmonic geometries occur between the Top Ilam and the Base Shahbazan reflectors, within the portion of the sedimentary sequence that was forming the first foredeep infill. This portion of the sequence is associated with the development of folds that appear to be partly decoupled from the underlying Ilam Formation (e.g. the small anticline to the SW of the Pataq Anticline) and with significant stratal thickness variations. The latter developed along with the local occurrence of growth geometries (e.g., to the NE of the Kerend Anticline), which suggests the existence of normal faults developed in the foredeep due to flexuring (e.g. Bradley and Kidd, 1991; Ranero et al., 2003; Tavani et al., 2015). Although the low quality of the seismic line would allow one to place both low- and high-angle NE-dipping faults below the Kerend anticline, the above described extensional growth geometry indicates that the step across the Kerend Anticline can be the result of the positive inversion of a pre-existing normal fault.

The two other sections here illustrated (i.e., sections 3 and 4) display features which are key for determining the structural style of the study area. Section 3 shows in detail the relationship between the Asmari and Gachsaran formations. The 20 to 30 km-wide gently SW-dipping monocline seen in section 1 projects to the location of three open anticlines occurring in the SW, central, and NE portions of the section. However, despite these three structures, the regional SW-dip is still recognisable. In the north-eastern syncline, reflectors of the Gachsaran Formation are parallel to the top of the Asmari Formation, whereas in the broad and gentle south-western syncline they are not. There, indeed, the Top Asmari forms a tighter syncline compared to reflectors within the Gachsaran and Agha Jari, mimicking a syn-kinematic geometry that, as mentioned for the seismic section 1, can be the result of the decoupling taking place within the evaporites of the Gachsaran Formation.

Section 4 (Fig. 3), which has been already published and discussed (Tavani et al., 2018b), includes three anticlines cored by the Garau Formation at the surface, which nearly project at the location of the Takhtgah Anticline seen in section 2. In details, these three anticlines are separated by two synclines cored by the Upper Cretaceous Gurpi Formation. The top of the Sehkanyian and Ilam formations are well marked in the seismic profile and are also well constrained from surface geology data. Reflectors ascribable to the Triassic and Paleozoic sedimentary succession are also recognisable. Overall, the structure illuminated in this section consists of two 10 km-wide monoclines bounding to the SW and to the NE a partly inverted graben. Evidence which suggests the inversion of an inherited graben include (Tavani et al., 2018b): (i) the fact that the elevation of the Sehkanyian Formation in the central syncline of the graben is lower than that at the borders of the two external monoclines, (ii) the continuity of reflectors within the monoclines which point to the occurrence of steeply dipping faults located at the edge of the graben.

4.2. Geological cross section

The geological cross section is shown in Fig. 4. It traverses the whole study area and is oriented nearly perpendicular to the main structural features of this part of the Zagros belt. In detail, starting from the lower stratigraphic levels, the stratigraphic package including the Cretaceous Garau, Sarvak and Ilam formations is buried along most of the section, with the exception of the NE part of the study area where it crops out in the hinge zone of some anticlines. Despite the evidence of thickness variations as derived from the analysis of the seismic section profiles (Fig. 3, Section 2), in the geological cross section the thickness of this package is drawn as constant for the sake of simplicity, and due to the lack of constraints in large portions of the sections. To the

north of the study area, where they are exposed, their cumulative thickness ranges from 400 to 2000 m, partly due to the variable accommodation space inherited from the Early Jurassic rifting (Tavani et al., 2018b). An average thickness of 700 m is used in the shallow section (and later in the balanced cross section) and the base of this package (i.e. the base of the Garau Formation) corresponds to the bottom of the geological cross-section.

Similarly, the thickness of the Gurpi Formation is roughly constant along most of the section (ca. 1100 m), except than immediately to the north of the Kerend Anticline, where, as also evident on seismic section 2 (Fig. 3), a local remarkable thickening of the formation occurs (Fig. 3). Also, to the south of the Vizehnan Anticline, the exposed short-wavelength anticlines affecting the Asmari Formation are assumed to be confined to within the Gurpi to Asmari package and to develop above the roughly SW-dipping top of the Ilam Formation. The stratigraphic package between the Gurpi and the Shahbazan formations, which includes the Pabdeh, Kashkan, Taleh Zang, and Amiran formations, prominently thins SW-ward, passing from a maximum thickness of 700 m to the NE of the Pataq Anticline to a minimum one of 400 m to the SW of the Mileh Sorkh Anticline. The cumulative thickness of the Shahbazan and Asmari formations is constant across the entire geological cross section and it is nearly 350 m.

In the SW part of the section, stratigraphically on top of the Asmari Formation, the evaporites of the Gachsaran Formation are partially decoupled from the underlying formation, mimicking syn-kinematic geometries, as already seen in the seismic reflection profiles 1 and 4 (Fig. 3), and as previously described in the literature for the Lurestan arc (Emami et al., 2010; Vergés et al., 2011b). There is also a tendency for the Gachsaran Formation to vary in thickness towards the more internal structures. In particular, surface data indicate a rather constant thickness in between the Darvana and Mileh Sorkh anticlines and a gradual thinning northward. For example, across the Mileh Sorkh anticline the thickness of the Gachsaran Formation strongly decreases. Furthermore, further to the NE (i.e. to the NE of the Kerend Anticline) the Gachsaran and the Agha Jari formations disappear and few patches of continental deposits, equivalent of the Bakhtiari Formation, directly rest on top of the Cretaceous to Miocene sequence. The northward thinning of the Gachsaran Formation suggests that the area to the NE of the Mileh Sorkh Anticline was already uplifted during the deposition of the Agha Jari Formation. To the SW, instead, strata of the Agha Jari and Gachsaran are parallel to one another, as seen in the seismic sections across the frontal portion of the study area (sections 1 and 3 in Fig. 3).

There is no available seismic section allowing to evaluate in detail the geometric relationship between the Agha Jari and the Bakhtiari formations, although at outcrops these formations are generally almost parallel to one another. Locally, however, growth geometries can be observed. An example of this is shown in Fig. 5, where gently SW-dipping strata of the Bakhtiari Formation seal a syncline which involves in the deformation the Agha Jari Formation along with the lowermost portion of the Bakhtiari Formation itself. This evidence indicates that the folding of the Agha Jari and of the lower portion of the Bakhtiari formations took place at an earlier stage than that responsible for the development of the large-scale tilting observed in the southern portion of the geological cross section (of which this exposure form par), which also involves the uppermost portion of the Bakhtiari Formation (Figs. 4 and 5). Finally, similarly to what can be seen in the seismic reflection section 2 (Fig. 3), the geological cross section indicates that: (i) with the exception of the High Zagros Fault, there is no remarkable exposed thrust in the area; (ii) the envelope of synclines indicates the occurrence of two structural steps located across the Kerend and the Takhtgah anticlines.

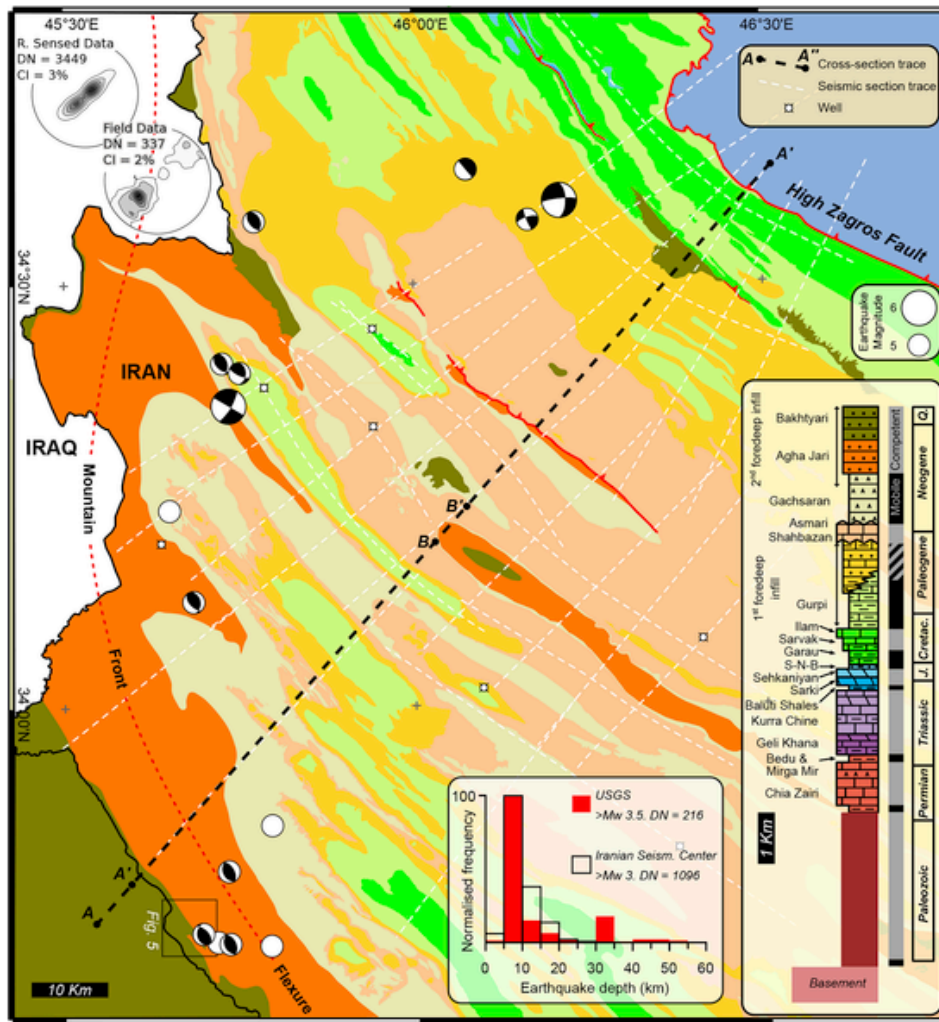


Fig. 4. NE-SW-oriented geological section (the trace is shown in Fig. 2), with (i) projected $M_w > 5$ earthquakes (projection distance < 25 km, depth sourced by USGS, <https://earthquake.usgs.gov>), and swat profiles with (ii) maximum (blue), minimum (red), and average (magenta) elevation. The section is split into two parts, with an overlap zone (B-B'). (For interpretation of the references to colour in this figure legend, the reader is referred to the Web version of this article.)

4.3. Geomorphic features

The studied area is elevated relative to adjacent sectors of the region (Fig. 1b), and underlines the regional water divide (Fig. 6a). Topography of the investigated area is influenced by the variable resistance to erosion of the outcropping rocks, with salients (e.g., anticlinal domes or hogbacks encircling breached anticlines) typically associated with the hard limestones of the Asmari Formation (e.g. Oberlander, 1965; Tucker and Slingerland, 1996; Burberry et al., 2007, 2010; Ramsey et al., 2008; Zebari et al., 2019).

The large-scale topographic features of the study area are synthesised in the swath profile of Fig. 4, and in the Mean elevation map of Fig. 6b. The swath profile of Fig. 4 condenses elevation data from a 30 km wide belt centred on the trace of cross section A'-A'' (location in Fig. 2) to a single profile. Comparison of the swath profile with the geological cross section (Fig. 4) shows that elevation curves are characterised by a net step marking a jump in elevation values at the location of the prominent Pataq Anticline, which only slightly diminish towards the NE, in the Zimakani River area (Fig. 4). When examined in map view (Fig. 6b), the spatial distribution of the mean elevation shows that values tend to increase from the boundary of the MFF towards the NE to attain the highest values (> c. 1700 m) in the area of the Pataq anticline and to the NE of it, in the area of the HZF.

The features of the fluvial network show that, consistent with the SW to NE topographic gradient, the southwestern part of the investigated area is drained by mainly SW-flowing, transverse rivers (Fig. 6a). Towards the NE, however, to the NE of the Vizehnan Anticline, the regional water divide is associated with a zigzag pattern with an overall SW-NE trend and the main rivers flow through longitudinal (i.e., NW-SE trending) valleys flanked by prominent carbonate ridges (Fig. 6a). In this region, the presence of wind gaps that incise the ridge crests, and elbows (Fig. 6a), are suggestive of drainage reorganization and river capture phenomena that could have been controlled by either base level fall or small/large scale uplift. The origin of the drainage reorganization remains unclear in the area spanning from the Vizehnan anticline, to the SW, to the Pataq anticline, to the NE. In that area both the features of the relief (which are strongly controlled by lithology) and, within it, of the valleys, which display concave bottoms and absence of fluvial terraces, point to the major role played by erosion in sculpting the topography. Conversely, in the region to the NE of the Pataq Anticline, the presence of several relic erosional landforms allow reconstruction of a multi-stage evolution of the land surface. The geomorphic elements that are significant to the reconstruction are an incised pediment, which is identified in the Zimakani River area (Fig. 6a), and the active and relic drainage net, which dissects the Kerend anticline and the elevated area to NE of it (Fig. 6c). In the Zi-

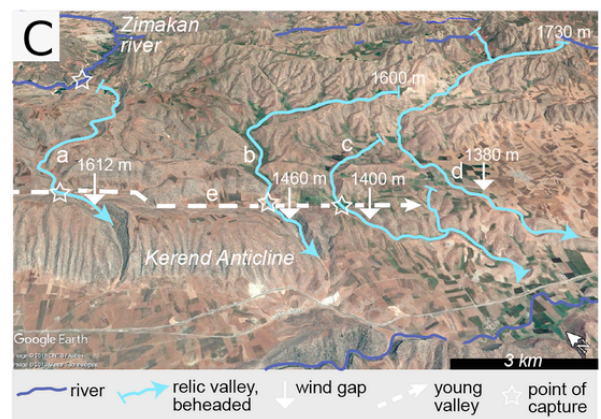
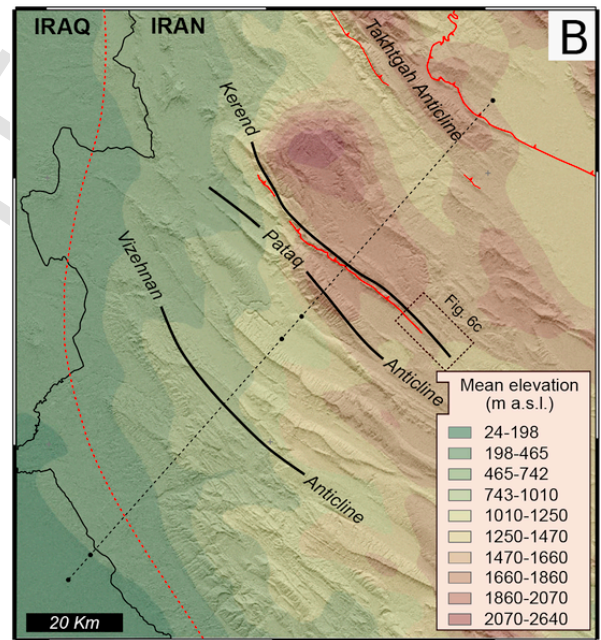
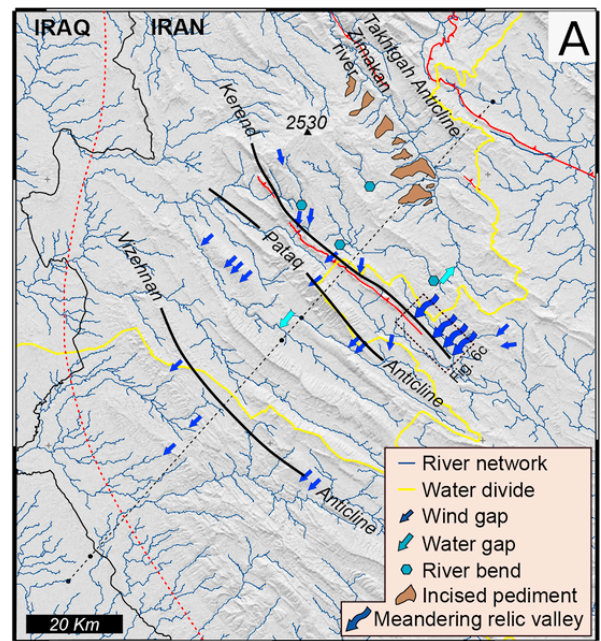
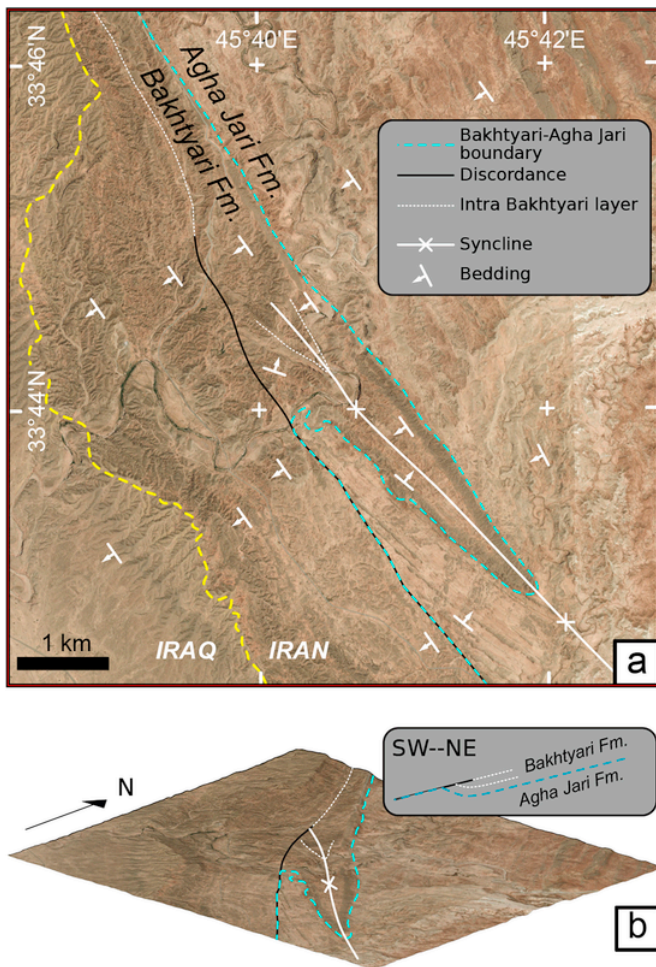


Fig. 5. SW-dipping strata of the Bakhtyari Formation sealing a syncline cored by the Agha Jari Formation (location shown in Fig. 2). (A) Orthophoto with structural scheme. (B) 3D view of the area in (A), seen from SE.

makán River area, an incised pediment gently dipping towards the NE, sculpted on the soft foredeep sediments (mostly shales and marls) and thus postdating erosion of the Asmari Formation, does occur (Fig. 2; Fig. 6a). The present-day drainage of the Kerend anticline and the elevated area to the NE of it is currently oriented towards both the NW (Zimakan River) and SE. The SE part of that region is incised by a relic drainage net that consists of a series of beheaded transverse valleys originally draining towards the SW, irrespective of the underlying folds (Fig. 6a). The transverse valleys are characterised by incised meanders (the highest ones, about 50 m deep, are located at around 1700 m a.s.l. along the dry valley a; Fig. 6c) that suggest the presence in that area of a low-gradient, SW-dipping land surface prior to the development of the topographic low in the Zimakan River area, and related beheading of valleys a and d of Fig. 6c. The orientations of the trunks of valleys a to d across the Kerend anticline systematically deviate from that of maximum steepness dictated by the fold flank (Fig. 6c). Such features may represent the response of the stream network to the development and lateral growth of that fold, as also shown in the SE Zagros (Ramsey et al., 2008; Walker et al., 2011).

4.4. Earthquake data

In the Lurestan region, the Mw 7.3 November 12, 2017 Ezgeleh earthquake was followed by more than 200 aftershocks with Mw > 4, which appear to be clustered in two main areas (Fig. 1b). The first area is located immediately to the west of the mainshock, and de-

Fig. 6. Main topographic and hydrographic features of the study area. (A) River network, with indication of the regional divide and main relic drainage and erosional features; the frame indicates location of diagram C. (B) Mean elevation map. (C) Google Earth view (3X vertical exaggeration) showing the relic drainage in the SE Kerend anticline. The occurrence of elbows (or points of capture) along valleys a, b, c and d paralleled by the wind gaps located at decreasing elevation from the NW to the SE along the Kerend anticline, indicate the abandonment of the transverse drainages a to d in favour the longitudinal valley e, possibly prior to capture by the Zimakan river, which flows to the NE (in the background).

finishes an about 150 km long N–S elongated ribbon positioned across the Mountain Front Flexure. The second area is located nearly 50 km to the SE of the mainshock. The focal mechanisms of several events with $M_w > 5$ are also available and indicate strike-slip and thrust kinematics for the faulting occurring within the study area, both characterised by nodal planes consistent with a shortening direction oriented NE–SW (Fig. 2). In particular, seven $M_w > 5$ earthquakes have occurred along the Mountain Front Fault system at a distance < 25 km from the geological cross section (Fig. 2). Focal mechanism data are available for four of these earthquakes, all of them being characterised by a reverse fault plane solution. These focal mechanism data have been projected on the geological cross section shown in Fig. 4, using the strike of the NE-dipping nodal plane as the projection direction (as it is consistent with the first order geometry of the Mountain Front Fault system). Three of these events project at a similar location and have a homogeneous nodal plane geometry. In detail, these events have hypocentral depths ranging between 13 and 14 km, project onto the section at a distance of 10–20 km south of the Darvana Anticline, and the dip of the NE-dipping nodal plane ranges between 30° and 45° . We here interpret these events to be the geometric and kinematic expression of the Mountain Front Fault system.

5. Balanced cross section

The geological cross section shown in Fig. 4 has been extended at depth by using the cross-section balancing technique (e.g. Dahlstrom, 1969; Hossack, 1979; Elliot, 1983). In detail, we have assumed flexural-slip folding (Donath and Parker, 1964) and preservation of bed thickness and line-length (Dahlstrom, 1969). In order to ease the computation of beds length, a homogeneous thickness is assumed

for all the stratigraphic units (whose values are provided in section 3.2), with the exception of the top Ilam to base Shahbazan interval for which we used 1500 m SW of the Mileh Sorkh Anticline and 1800 m NE of the Pataq Anticline. For the deeper portion of the section not shown in Fig. 4, we have used thickness values consistent with Tavani et al. (2018a). In particular, a total thickness of 1350 m is assumed for the Triassic to Middle Jurassic sequence (i.e. from the base of the Geli Khana Formation to the base of the Garau Formation), which is well constrained by outcrop data from the immediate north of the study area (Tavani et al., 2018b). Thicknesses of 1 km for the Permian and 3 km for the pre-Permian sedimentary sequence are here used, which are also consistent with the observed depth of the base of the sedimentary sequence as observed in the seismic reflection sections presented in this article (Fig. 3). Finally, in agreement with the occurrence of a seismic gap between 20 and 30 km depth (Fig. 2), we estimated a thickness of 11 km for the basement comprised between the base of the sedimentary sequence and the top of the ductile middle crust level. Such an inference being in agreement with previous work in the area (e.g. Talebian and Jackson, 2004; Nissen et al., 2011). Our balanced cross section, along with its restoration, is shown in Fig. 7.

The Shahbazan to Asmari stratigraphic package is reconstructed along the entire section, also to the NE of the Takhtgah Anticline where there is no evidence that it was deposited. This was done as this package represents the best constrained portion of the multilayer, and we therefore took its length as a reference for cross section balancing. The present day length of the section is 134.2 km, whereas the unfolded and unfaulked length of the Shahbazan to Asmari package is 140.4 km, implying a shortening of 6.2 km. Surface geology data and the interpretation of seismic reflection profiles evidence some decoupling between competent and mobile packages, with folds having wavelengths of less than 5 km being confined to different portions of the sedimentary cover. Furthermore, the integration of surface geology, borehole data, and interpretation of seismic reflection profiles, indicates the occurrence of thrusts (underneath the Vizehnan, Mileh Sorkh, and Kerend Anticline) and backthrusts (SE of the Pataq Anticline). There is however, no evidence of large displacement associated with neither of them. The necessity for preserving line-length is also suggestive of very limited displacements associated with the thrust faults. Therefore,

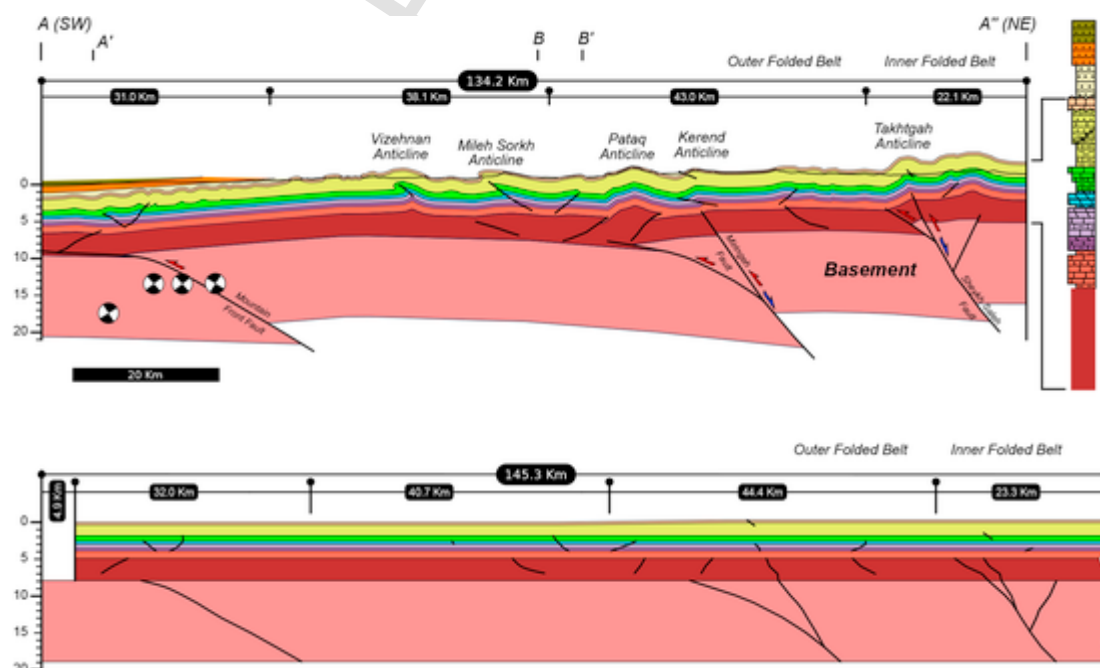


Fig. 7. Balanced cross section along the direction of the geological section in Fig. 4, and restored section. The stratigraphic succession shown in Fig. 2 is also illustrated.

we confined them to within Mesozoic structural levels. Some low displacement thrusts are also assumed to occur within the Paleozoic sequence. The occurrence of deeply located thrusts are a geometric requirement for maintaining the length of the Paleozoic layers equal to that of the Meso-Cenozoic ones. In agreement with the geometries observed in the seismic reflection sections (Fig. 3), the two basement steps observed in the seismic section 2 of Fig. 3 and inferred in the geological cross section of Fig. 4, i.e. the steps across the Kerend (Step 1) and Takhtgah (Step 2) anticlines, are here interpreted as the result of the positive inversion of deeply rooted inherited extensional faults. A foot-wall shortcut occurs along both inverted faults. The interpretation of these two steps as inverted normal faults also fits with the extremely low amount of shortening observed in the Meso-Cenozoic stratigraphic sequence. In our reconstruction, structures affecting the Paleozoic to Cenozoic sedimentary succession between the Vizehnan and Takhtgah anticlines accommodated shortening transferred to the cover by the Sheikh Saleh and Miringeh inverted faults (Fig. 7). No major structures affecting the cover occurs to the SW of the Vizehnan Anticline, where shortening in the Asmari Formation is nearly 1 km.

Scaling relationships between down-dip rupture and earthquake magnitude (e.g. Wells and Coppersmith, 1994) indicate that the $M_w > 5$ events projected onto the section should have occurred along faults having a cross sectional length exceeding 3 km. The clustering of these events suggests that these faults form patches located along the main strand on the Mountain Front Fault system. Notably, the Mountain Front Fault system is located at the southwestern edge of the large anticlinorium that starts from the Kerend Anticlines and ends in the foredeep region.

The reconstructed geometry of the section implies a different amount of shortening for the basement and the sedimentary cover, the latter needing almost 5 km of additional shortening to occur SW of the section. The High Zagros Fault, which occurs in the NE portion of the section (Fig. 4), is not included in the balanced cross section for the sake of simplicity.

6. Discussion

6.1. Tectonic style and comparison with previous studies

The balanced cross section illustrated in Fig. 7 is almost entirely confined to within the outer Zagros folded belt, which in the study area appears to be associated with a hybrid deformation style. This composite tectonic style includes inversion tectonics and “pure” thrusting, in the central and NE, and in the SW portions of the balanced cross section, respectively.

In detail, in our reconstruction a slightly transported crustal-scale fault propagation fold is associated with the Mountain Front Fault. Such a scenario is constrained by the location of the hypocentres of the $M_w > 5$ earthquakes associated with the aftershock sequence of the $M_w 7.3$, November 12, 2017, earthquake that hit the Zagros belt in the Lurestan region (Figs. 1b and 4). These hypocentres, indeed, are located a few km to the NE of the trailing syncline of the crustal-scale anticline (Fig. 4), rather than underneath the crest-forelimb transition of this anticline (i.e. below the Vizehnan Anticline) as would be required by a fault-bend folding solution (in which the ramp underlies the crest). On the other hand, the inversion tectonics style adopted in the central and NE portions of the section is consistent with the structures imaged in the seismic reflection profiles (Fig. 3), and it is also a geometric requirement minimising the amount of shortening within the basement. This, in turn, serves as a mechanism for producing significant uplift in the interior of the folded belt without transferring an excessive amount of shortening to its foreland. In our section, the shortening transferred to the foreland is < 5 km, in line or below the values adopted by other authors in the same area (Fig. 8). This value is compatible with the scarce shortening observed in the foreland region (Fig. 8f) and it

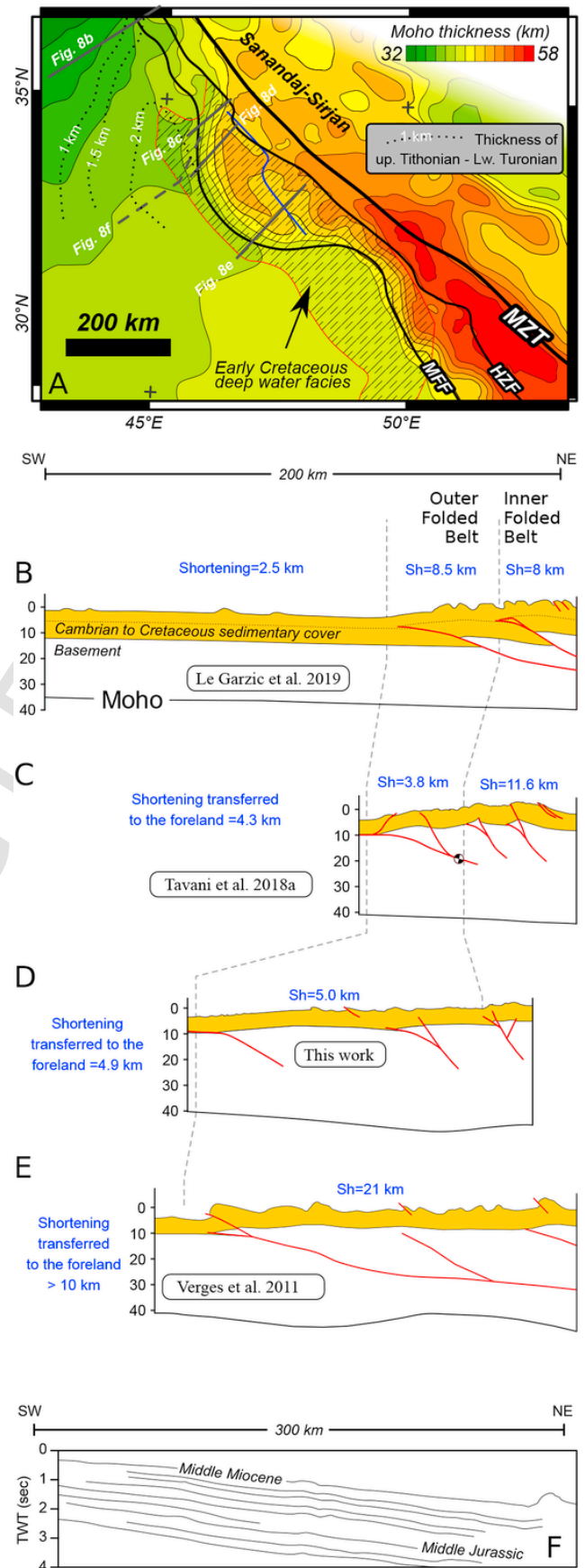


Fig. 8. (A) Moho thickness in the Lurestan arc and surrounding zones (after Jiménez-Munt et al., 2012), with extent of Early Cretaceous deep-water facies indicated (after Ziegler, 2001), and thickness of the upper Tithonian - lower Turonian sequence (after English et al., 2015). (B-E) Schematic crustal scale cross sections across the Kirkuk embayment and the Lurestan arc, with Moho indicated. The Moho in sections B-D is from Jiménez-Munt et al., 2012, in section (E) it is redrawn from Paul et al. (2010). (F) Line drawing of a seismic section across the foreland area (after Mohammed, 2006).

could have been easily accommodated by meso-scale structures, such as tectonic stylolites or mesoscopic folds, which are widespread in the Mesozoic and Cenozoic multilayer of the Lurestan region (Tavani et al., 2018c). The amount of shortening for the sedimentary cover along the section can be estimated to be nearly 6 km, corresponding to about 5% of its original length. Several balanced cross sections have been provided in the literature for the whole Zagros mountain belt, which indicate up to 25% total shortening (Molinari et al., 2005; Mouthereau et al., 2006; Allen et al., 2013; Bigi et al., 2018), including estimates for the Lurestan area (Blanc et al., 2003; Vergés et al., 2011a). However, most of this total shortening is thought to be accommodated by the High Zagros Fault (e.g. Vergés et al., 2011a) and published shortening values that exclusively take into account deformation associated with the folded belt are more in line with the results presented in this work. For example, balanced cross sections across the Lurestan arc (Vergés et al., 2011a; Tavani et al., 2018a) and the Kirkuk embayment (Le Garzic et al., 2019) suggest an amount of shortening in the sedimentary cover of the folded belt of nearly 15–20 km (Fig. 8). Furthermore, when considering only the shortening accommodated in the outer part of the folded belt, our reconstruction (~6 km of shortening) becomes consistent with the information from the NW Lurestan arc (~4 km of shortening, Tavani et al., 2018a, Fig. 8c) and from the Kirkuk embayment (8 km of shortening, Le Garzic et al., 2019, Fig. 8b. 5% of shortening according to Obaid and Allen, 2017).

In agreement with the seismic gap observed between 20 and 30 km depth (Fig. 2) (already illuminated by Nissen et al., 2011) and consistently with previous works in the Zagros (e.g. Mouthereau et al., 2006; Vergés et al., 2011a), we infer thrust and inverted normal faults sole down into a mid-crustal ductile detachment level.

Concerning the timing of deformation, the northeastward thinning of the Gachsaran Formation across the Mile Sorkh and Kerend anticlines (e.g. Fig. 4) indicates that the NE portion of the section uplifted earlier than the SW one, probably already during the late Miocene. Early uplift of the area spanning from the Pataq anticline to the HZF relative to the region to the SW of it is also inferred from the river network features. In fact, paleo-flow orientations and valley beheading phenomena suggest the occurrence, in the area spanning from the Kerend anticline to the Takhtgah Anticline (Fig. 6), of an elevated land surface gently dipping towards the SW eroded in the Asmari Formation carbonates possibly coeval with folding, as it is inferred from the features of the relic drainage in the SE Kerend anticline. The SW-dipping elevated surface predates a first stage of river incision (with related stream capture) and surface lowering in the Zimakan River area, which nowadays exhibits high mean elevation values despite the presence of weak lithology at the surface. Further deepening of the Zimakan River valley that postdates formation of the pediment, suggests a second stage of uplift, which could be related with the more recent activity of the Mountain Front Fault. In the NW portion of the Lurestan arc, onset of cover folding in the Mountain Front Flexure area is dated at about 8 Ma (Homke et al., 2004), i.e. syn Agha Jari. This is consistent with the reduced thickness of the Gachsaran Formation observed in the northern portion of the geological cross section (Fig. 4), which suggests post-depositional uplift and erosion of the Gachsaran Formation. However, tilting of a fold-sealing unconformity in the Bakhtiari Formation during the flexure development (Fig. 5), indicates that folding within the cover sequence and the onset of the Mountain Front Flexure

were not coeval. In particular, such a feature shows that the development of the Mountain Front Flexure, and thus the development of the Mountain Front Fault system in the study area, can be traced back to approximately after 3 Ma (i.e. the age of the base of the Bakhtiari Formation; Homke et al., 2004). This is in agreement with Koshnaw et al. (2017) that, based on low-temperature thermochronology data, suggest a similar 5 ± 1 Ma age for the onset of the Mountain Front Fault system activity in the NW Zagros.

In summary, the study area is characterised by a hybrid style of deformation, in which folding of the cover sequence and inversion tectonics in the basement occurred together, in a piggy back propagation sequence. Later, during the final stages of shortening, the basement-involving, gently dipping Mountain Front Fault developed at the toe of the belt.

6.2. Early Jurassic inheritances and their influence in determining the sinuities of the frontal Zagros belt

The structural architecture of a number of mountain belts worldwide, and in particular that of their foreland, has been shown to be largely affected by several modes of re-use of pre-existing basement faults inherited from the rifted margin (e.g. Williams et al., 1989; Cooper et al., 1989; Coward et al., 1991; Mazzoli et al., 2005; Camanni et al., 2016; Brown et al., 2017; Granado et al., 2017). In particular, it has been demonstrated that pre-existing basin-bounding extensional faults can be positively inverted during mountain building processes (Carrera et al., 2006; Tavani et al., 2013; Camanni et al., 2014a,b), and that the structural complexity of the fault systems in the basement may locally force the development of bends in the structural trend of an otherwise roughly straight, overlying fold and thrust belt (Macedo and Marshak, 1999; Jammes et al., 2014; Tugend et al., 2014; Alvarez-Marron et al., 2014; Szaniawski et al., 2017). In the structural model that we present in this work for the foreland of the Zagros belt, the Mountain Front Fault system appears to correspond to a late stage, gently NE-dipping crustal thrust that developed at the leading edge of an array of steeply dipping, positively inverted extensional faults. Structural inheritances associated with the rift architecture could be, therefore, suitable candidates for explaining both structure and sinuities of the Mountain Front Fault system also in the Zagros belt.

As already briefly mentioned, the Lurestan region underwent a major extensional pulse during the Early Jurassic, which resulted in the development of NW-SE oriented troughs (Tavani et al., 2018b) and in the shift of the depositional environment of a large area from shallow to deep-water (e.g. Koop and Stoneley, 1982; Ziegler, 2001; Barrier and Vrielynck, 2008). Extension and development of Early Jurassic basins required thinning of the crust in a widespread area, which was underfilled during the Middle and Late Jurassic. The map distribution of the overlying Early Cretaceous deep-water facies can be therefore used as a proxy for defining the rough shape of the area that experienced Early Jurassic crustal thinning. This area is overall oriented NW-SE and its south-western border nearly coincides with the location of the Mountain Front Flexure (Fig. 8a), suggesting that the development of the Mountain Front Flexure is somewhat linked to the re-use of pre-existing fault systems that controlled the deposition of Middle Jurassic to Early Cretaceous deep water facies. On the other hand, the relatively sudden NW-ward termination of Jurassic and Cretaceous deep water facies across the boundary between the Lurestan arc and the Kirkuk embayment, along with the NW-ward thinning of the Tithonian-Turonian sequence (Fig. 8a), can be attributed to the Jurassic rift segmentation and in particular to the occurrence of NE-SW oriented faults or to inherited crustal scale N-S striking faults, which are widely documented in the Arabian Plate (e.g. Falcon, 1974; Talbot and Alavi, 1996; Hessian et al., 2001).

Consistently with the lateral rift segmentation, despite the strong compressional overprint which has altered the original crustal thickness, the Moho depth below the Lurestan arc shows evidence of Jurassic NE-ward crustal thinning, which instead does not occur in the Kirkuk embayment, suggesting the lateral juxtaposition of different Early Jurassic rift domains. The sections across the Kirkuk embayment and the NW portion of the Lurestan arc (Fig. 8b and c) are characterised by a rather linear increase of the Moho depth from SW to NE. Conversely, the two sections across the central part of the Lurestan Arc (Fig. 8d and e) are characterised by a region of crustal thinning, located immediately to the NE of the Mountain Front Fault system. This thinned area, when observed in map view, defines two NW-SE elongated regions (marked by the blu line in Fig. 8a), which could correspond to regional graben structures.

All the above described features suggest a key role of the Early Jurassic rift structure in shaping the Mountain Front Flexure and in determining its sinuosity in the western portion of the Lurestan arc. In detail, according to our interpretation, the pre-orogenic architecture of the Arabian margin in the NW portion of the Lurestan arc was defined by NW-SE elongated extensional domains, with secondary N-S to NE-SW striking fault systems segmenting the proximal domain of the margin (Fig. 9a). The Mountain Front Fault system, and thus the flexure, developed with a sinusoidal shape that follows the boundary between the Jurassic thinned (and drowned) crust and the area that did not experienced remarkable thinning and dronwnig during Jurassic rifting. In essence, the Mountain Front Flexure follows the trend of the laterally segmented boundary between the Jurassic proximan and necking domains of the margin (Fig. 9b).

As the Mountain Front Fault system is not an inherited fault but, rather, it is a newly generated fault rooted in the middle to lower crust, the reason for the parallelism between the Mountain Front Fault system and extensional domains should be found in the inherited architecture and rehology of the deep crustal levels of the passive margin. In particular, as pointed out by several authors (e.g. Cloetingh et al., 2005; Sutra et al., 2013; Lacombe and Bellahsen, 2016; Lescoutre, 2019), thinning of the crust during rifting and its subsequent cooling significantly reduces the rock volumes that can undergo deformation by ductile processes. Consequently, the weak zones in the middle and lower crust thins oceanward and, eventually, in the distal domains

of rift systems almost the entire crust shows a brittle behaviour and becomes coupled with the mantle (Sutra et al., 2013). We speculate that, in the distal portions of the Arabian margin, the mid-crustal ductile layer is not well developed. Therefore, it cannot provide a suitable weakness level for the activation of a large and interconnected basal detachment.

Conversely, in the innermost portion of the necking domain and in the proximal domain, the ductile middle crust layer is thick and well developed, and may therefore provide a significant mechanical weakness for the development of detachment levels. Accordingly, in the Lurestan arc of the Zagros belt, efficient decoupling along a mid-crustal basal decollement occurred as the study area became involved in deformation. This allowed for the development of a the fontal thrust that mimics the trend of the basin boundary.

7. Conclusions

In this work, we have integrated information from near-vertical seismic reflection profiles, surface geology, geomorphic, and earthquake data to build a balanced cross section across the NW portion of the Lurestan arc. The amount of shortening in the section does not exceed 10 km, with partial decoupling between the sedimentary cover and the basement. In our reconstruction, the Mountain Front Flexure is the frontal limb of a crustal-scale, slightly transported, fault propagation anticline, associated with the NE-dipping Mountain Front Fault. Such a fault developed as a late stage structure and splays off from a mid-crustal decollement level, ahead of a system of positively inverted normal faults. Our study suggests a strong control of the Early Jurassic rift architecture on the structure of the belt. In particular, the Mountain Front Fault nucleates in the inner portion of the necking domain of the Jurassic rift, where the mid-crustal ductile level is sufficiently thick to promote the development of a large and interconnected decollement, from which the Mountain Front Fault emanates. Lateral segmentation of the Jurassic rift, accommodated by transfer faults, promoted a differential advancement of the necking domain between the Kirkuk embayment and the Lurestan arc, which resulted in the sinusoidal shape of the Mountain Front Fault and in its different position in the two regions.

Uncited references

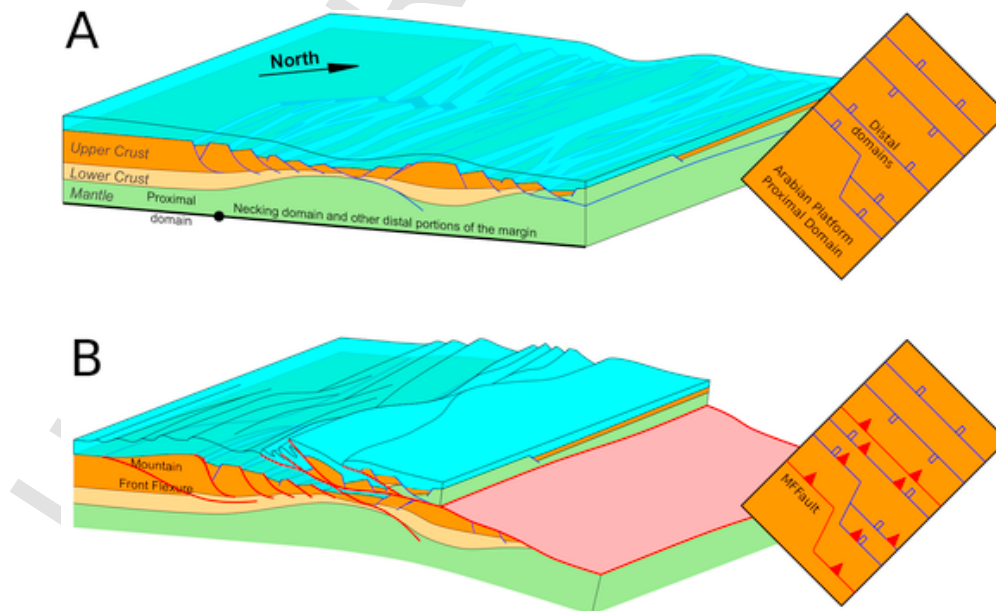


Fig. 9. 3D scheme and map view showing the evolution of the Lurestan arc-Kirkuk embayment boundary region. (A) End of Early Jurassic rifting. (B) Development of the Mountain Front Fault during the Plio-Pleistocene. See text for details.

CRedit authorship contribution statement

Tavani Stefano: Conceptualization, Investigation, Writing - original draft, Writing - review & editing. **Camanni Giovanni:** Writing - review & editing, Validation. **Nappo Michele:** Data curation, Visualization. **Snidero Marco:** Data curation, Visualization. **Ascione Alessandro:** Data curation, Validation. **Valente Ettore:** Formal analysis. **Gharabeigli Gholamreza:** Funding acquisition, Investigation. **Morsalnejad Davoud:** Funding acquisition, Investigation. **Mazzoli Stefano:** Project administration, Writing - review & editing, Conceptualization.

Declaration of competing interest

The authors declare that they have no known competing financial interests or personal relationships that could have appeared to influence the work reported in this paper.

Acknowledgments

Midland Valley is thanked for providing the Move software (Academic License to the University of Naples Federico II). We acknowledge the use of imagery from the Land Atmosphere Near-real time Capability for EOS (LANCE) system, operated by the NASA/GSFC Earth Science Data and Information System (ESDIS) (<https://earthdata.nasa.gov/>) with funding provided by NASA/HQ. Authors thank Mark Allen and an anonymous reviewers for their constructive criticisms and suggestions. We also thank F. Puzone for technical support during seismic interpretation. Requests for obtaining the near-vertical seismic section should be submitted to the National Iranian Oil Company. All the other data used in this work are listed in the references.

References

- Alavi, M., 1980. Tectonostratigraphic evolution of the Zagrosides of Iran. *Geology* 8, 144–149. doi:10.1130/0091-7613(1980)8<144:TEOTZO>2.0.CO;2.
- Alavi, M., 1991. Sedimentary and structural characteristics of the Paleo-Tethys remnants in northeastern Iran. *Geol. Soc. Am. Bull.* 103, 983–992. doi:10.1130/0016-7606(1991)103<0983:SASCOT>2.3.CO;2.
- Alvarez-Marron, J., Brown, D., Camanni, G., Wu, Y.-M., Kuo-Chen, H., 2014. Structural complexities in a foreland thrust belt inherited from the shelf-slope transition: insights from the Alishan area of Taiwan. *Tectonics* 33, 1322–1339.
- Bradley, D.C., Kidd, W.S.F., 1991. Flexural extension of the upper continental crust in collisional foredeeps. *Geol. Soc. Am. Bull.* 103, 1416–1438. doi:10.1130/0016-7606(1991)103<1416:FEOUC>2.3.CO;2.
- Brown, D., Alvarez-Marron, J., Biete, C., Kuo-Chen, H., Camanni, G., Ho, C.W., 2017. How the structural architecture of the Eurasian continental margin affects the structure, seismicity, and topography of the south central Taiwan fold-and-thrust belt. *Tectonics* 36, 1275–1294.
- Macedo, J., Marshak, S., 1999. Controls on the geometry of fold-thrust salients. *Geol. Soc. Am. Bull.* 111, 1808–1822. doi:10.1130/0016-7606(1999)111<1808:COTGOF>2.3.CO;2.
- Agard, P., Omrani, J., Jolivet, L., Mouthereau, F., 2005. Convergence history across Zagros (Iran): constraints from collisional and earlier deformation. *Int. J. Earth Sci.* 94, 401–419. doi:10.1007/s00531-005-0481-4.
- Alavi, M., 1994. Tectonics of Zagros orogenic belt of Iran, new data and interpretation. *Tectonophysics* 229, 211–238. doi:10.1016/0040-1951(94)90030-2.
- Alavi, M., 2007. Structures of the Zagros fold-thrust belt in Iran. *Am. J. Sci.* 307, 1064–1095. doi:10.2475/09.2007.02.
- Allen, M.B., Armstrong, H.A., 2008. Arabia–Eurasia collision and the forcing of mid-Cenozoic global cooling. *Palaeogeogr. Palaeoclimatol. Palaeoecol.* 265, 52–58. doi:10.1016/j.palaeo.2008.04.021.
- Allen, M.B., Talebian, M., 2011. Structural variation along the Zagros and the nature of the Dezful embayment. *Geol. Mag.* 148, 911–924. doi:10.1017/S0016756811000318.
- Allen, M.B., Saville, C., Blanc, E.P., Talebian, M., Nissen, E., 2013. Orogenic plateau growth: expansion of the Turkish-Iranian Plateau across the Zagros fold-and-thrust belt. *Tectonics* 32, 171–190. doi:10.1002/tect.20025.
- Bahroudi, A., Koyi, H., 2003. Effect of spatial distribution of Hormuz salt on deformation style in the Zagros fold and thrust belt: an analogue modelling approach. *J. Geol. Soc.* 160, 719–733. doi:10.1144/0016-764902-135.
- Barber, D.D., Stockli, D.F., Horton, B.K., Koshnaw, R.L., 2018. Cenozoic exhumation and foreland basin evolution of the Zagros orogen during Arabia-urasia collision, western Iran. *Tectonics* 37, 4396–4420. doi:10.1029/2018TC005328.
- Barrier, E., Vrielynck, B., 2008. Paleotectonic Maps of the Middle East: Atlas of 14 Maps. Middle East Basin Evolution (MEBE) Programme.
- Berberian, M., 1995. Master “blind” thrust faults hidden under the Zagros folds: active basement tectonics and surface morphotectonics. *Tectonophysics* 241, 193–224. doi:10.1016/0040-1951(94)00185-C.
- Berberian, M., King, G.C.P., 1981. Towards a paleogeography and tectonic evolution of Iran. *Can. J. Earth Sci.* 18, 210–265. doi:10.1139/e81-019.
- Bigi, S., Carminati, E., Aldega, L., Trippetta, F., Kavosi, M.A., 2018. Zagros fold and thrust belt in the Fars province (Iran) I: control of thickness/rheology of sediments and pre-thrusting tectonics on structural style and shortening. *Mar. Petrol. Geol.* 91, 211–224. doi:10.1016/j.marpetgeo.2018.01.005.
- Blanc, E.P., Allen, M.B., Inger, S., Hassani, H., 2003. Structural styles in the Zagros simple folded zone, Iran. *J. Geol. Soc.* 160, 401–412. doi:10.1144/0016-764902-110.
- Bordenave, M.L., 2008. The origin of the Permo-Triassic gas accumulations in the Iranian Zagros Fold belt and contiguous offshore areas: a review of the palaeozoic petroleum system. *J. Petrol. Geol.* 31, 3–42. doi:10.1111/j.1747-5457.2005.tb00087.x.
- Braud, J., 1987. La suture du Zagros au niveau de Kermanshah (Kurdistan Iranien): Reconstitution paléogéographique, évolution géodynamique, magmatique et structural. PhD thesis, Université Paris-Sud.
- Bretis, B., Bartl, N., Grasmann, B., 2011. Lateral fold growth and linkage in the Zagros fold and thrust belt (Kurdistan, NE Iraq). *Basin Res.* 23, 615–630. doi:10.1111/j.1365-2117.2011.00506.x.
- Burberry, C.M., Cosgrove, J.W., Liu, J.G., 2007. Stream network characteristics used to infer the distribution of fold types in the Zagros Simply Folded Belt, Iran. *Journal of Maps*, Student Edition 32–45. doi:10.1080/jom.2007.9711027.
- Burberry, C.M., Cosgrove, J.W., Liu, J.G., 2010. A study of fold characteristics and deformation style using the evolution of the land surface: Zagros Simply Folded Belt, Iran. *Geological Society, London, Special Publications* 330, 139–154. doi:10.1144/SP330.8.
- Buscher, J.T., Ascione, A., Valente, E., 2017. Decoding the role of tectonics, incision and lithology on drainage divide migration in the Mt. Alpi region, southern Apennines, Italy. *Geomorphology* 276, 37–50. doi:10.1016/j.geomorph.2016.10.003.
- Camanni, G., Brown, D., Alvarez-Marron, J., Wu, Y.-M., Chen, H.-A., 2014. The Shuilikeng fault in the central Taiwan mountain belt. *J. Geol. Soc.* 171, 117–130.
- Camanni, G., Chen, C.-H., Brown, D., Alvarez-Marron, J., Wu, Y.-M., Chen, H.-A., Huang, H.-H., Chu, H.-T., Chen, M.-M., Chang, C.-H., 2014. Basin inversion in central Taiwan and its importance for seismic hazard. *Geology* 42, 147–150. doi:10.1130/G35102.1.
- Camanni, G., Alvarez-Marron, J., Brown, D., Ayala, C., Wu, Y.-M., Hsieh, H.-H., 2016. The deep structure of south-central Taiwan illuminated by seismic tomography and earthquake hypocenter data. *Tectonophysics* 679, 235–245.
- Carrera, N., Muñoz, J.A., Sàbat, F., Mon, R., Roca, E., 2006. The role of inversion tectonics in the structure of the Cordillera Oriental (NW Argentinean Andes). *J. Struct. Geol.* 28, 1921–1932. doi:10.1016/j.jsg.2006.07.006.
- Casciello, E., Vergés, J., Saura, E., Casini, G., Fernández, N., Blanc, E.P., Homke, S., Huntet, D.W., 2011. Fold patterns and multilayer rheology of the Lurestan Province, Zagros simply folded belt (Iran). *J. Geol. Soc.* 166, 947–959. doi:10.1144/0016-76492008-138.
- Casini, G., Casciello, E., Saura, E., Vergés, J., Fernandez, N., Hunt, D.W., 2018. Fracture characterization in sigmoidal folds: insights from the Siah Kuh anticline, Zagros, Iran. *AAPG (Am. Assoc. Pet. Geol.) Bull.* 102, 369–399. doi:10.1306/0503171615817076.
- Chen, K., Xu, W., Mai, P.M., Gao, H., Zhang, L., Ding, X., 2018. The 2017 Mw 7.3 Sarpol Zahāb Earthquake, Iran: a compact blind shallow-dipping thrust event in the mountain front fault basement. *Tectonophysics* 747, 108–114.
- Cloetingh, S., Ziegler, P., Beekman, F., Andriessen, P., Matenco, L., Bada, G., Garcia-Castellanos, D., Hardebol, N., Dezes, P., Sokoutis, D., 2005. Lithospheric memory, state of stress and rheology: neotectonic controls on Europe’s intraplate continental topography. *Quat. Sci. Rev.* 24, 241–304. doi:10.1016/j.quascirev.2004.06.015.
- Cooper, M.A., Williams, G.D., De Graciansky, P.C., Murphy, R.W., Needham, T., De Paor, D., Stoneley, R., Todd, S.P., Turner, J.P., Ziegler, P.A., 1989. Inversion tectonics—a discussion. *Geological Society of London, Special Publications* 44, 335–347. doi:10.1144/GSL.SP.1989.044.01.18.
- Coward, M.P.A., Gillcrist, R., Trudgill, B., 1991. In: *Extensional Structures and Their Tectonic Inversion in the Western Alps*, 56. Geological Society of London, Special Publication, pp. 51–77. doi:10.1144/GSL.SP.1991.056.01.07.
- Dahlstrom, C.D.A., 1969. Balanced cross sections. *Can. J. Earth Sci.* 6, 743–757. doi:10.1139/e69-069.
- Dercourt, J., Zonenshain, L.P., Ricou, L.-E., Kazmin, V.G., Le Pichon, X., Knipper, A.L., Grandjacquet, C., Sbertshikov, I.M., Geysant, J., Lepvrier, C., Pecheurs, D.H., 1986. Geological evolution of the Tethys belt from the Atlantic to the Pamirs since the Lias. *Tectonophysics* 123, 241–315. doi:10.1016/0040-1951(86)90199-X.
- Donath, F.A., Parker, R.B., 1964. Folds and folding. *Geol. Soc. Am. Bull.* 75, 45–62.
- Google earth <https://earth.google.com/web2019>
- Elliot, D., 1983. The construction of balanced cross-sections. *J. Struct. Geol.* 5, 101. doi:10.1016/0191-8141(83)90035-4.
- Emami, H., Vergés, J., Nalpas, T., Gillespie, P., Sharp, I., Karpuz, R., Blanc, E.P., Goodarzi, M.G.H., 2010. Structure of the mountain front flexure along the Anaran anticline in the Pusht-e Kuh arc (NW Zagros, Iran): insights from sand box models. *Geological Society of London, Special Publications* 330, 155–178. doi:10.1144/SP330.9.
- English, J.M., Lunn, G.A., Ferreira, L., Yacu, G., 2015. Geological evolution of the Iraqi Zagros, and its influence on the distribution of hydrocarbons in the Kurdistan region. *AAPG (Am. Assoc. Pet. Geol.) Bull.* 99, 231–272. doi:10.1306/06271413205.
- Falcon, N.L., 1961. Major earth-flexuring in the Zagros mountains of south-west Iran. *Q. J. Geol. Soc.* 117, 367–376. doi:10.1144/gsjgs.117.1.0367.
- Falcon, N.L., 1974. Southern Iran: Zagros mountains. *J. Geol. Soc.* 4, 199–211. doi:10.1144/GSL.SP.2005.004.01.11.
- Fernández, O., 2005. Obtaining a best fitting plane through 3D georeferenced data. *J. Struct. Geol.* 27, 855–858. doi:10.1016/j.jsg.2004.12.004.

- Ghasemi, A., Talbot, C.J., 2006. A new tectonic scenario for the Sanandaj-Sirjan Zone (Iran). *J. Asian Earth Sci.* 26, 683–693. doi:10.1016/j.jseas.2005.01.003.
- Gombert, B., Duputel, Z., Shabani, E., Rivera, L., Jolivet, R., Hollingsworth, J., 2019. The impulsive source of the 2017 (MW = 7.3) Ezgeleh, Iran, earthquake. *Geophys. Res. Lett.* 46, 5207–5216. doi:10.1029/2018GL081794.
- Granado, P., Ferrer, O., Muñoz, J.A., Thöny, W., Strauss, P., 2017. Basin inversion in tectonic wedges: insights from analogue modelling and the Alpine-Carpathian fold-and-thrust belt. *Tectonophysics* 703–704, 50–68. doi:10.1016/j.tecto.2017.02.022.
- Hessami, K., Koyi, H.A., Talbot, C.J., 2001. The significance of strike-slip faulting in the basement of the Zagros fold and thrust belt. *J. Petrol. Geol.* 24, 5–28. doi:10.1111/j.1747-5457.2001.tb00659.x.
- Homke, S., Vergés, J., Garcés, M., Emami, H., Karpuz, R., 2004. Magnetostratigraphy of Miocene-Pliocene Zagros foreland deposits in the front of the Push-e Kush arc (Lurestan province, Iran). *Earth Planet. Sci. Lett.* 225, 397–410. doi:10.1016/j.epsl.2004.07.002.
- Homke, S., Vergés, J., Serra-Kiel, J., Bernaola, G., Sharp, I., Garcés, M., Montero-Verdú, I., Karpuz, R., Goodarzi, M.H., 2009. Late Cretaceous–Paleocene formation of the proto-Zagros foreland basin, Lurestan province, SW Iran. *Geol. Soc. Am. Bull.* 121, 963–978. doi:10.1130/B260351.1.
- Hossack, J.R., 1979. The use of balanced cross-sections in the calculation of orogenic contraction: a review. *J. Geol. Soc.* 136, 705–711.
- James, G.A., Wynd, J.G., 1965. Stratigraphic nomenclature of Iranian Oil Consortium agreement area. *AAPG (Am. Assoc. Pet. Geol.) Bull.* 49, 2182–2245.
- Jammes, S., Huisman, R.S., Muñoz, J.A., 2014. Lateral variation in structural style of mountain building: controls of rheological and rift inheritance. *Terra. Nova* 26, 201–207. doi:10.1111/ter.12087.
- Jassim, S.Z., Goff, J.C., 2006. *Geology of Iraq*. Brno, Czech Republic: DOLIN, Distributed. Geological Society of London.
- Jiménez-Munt, I., Fernández, M., Saura, E., Vergés, J., García-Castellanos, D., 2012. 3-D lithospheric structure and regional/residual Bouguer anomalies in the Arabia-Eurasia collision (Iran). *Geophys. J. Int.* 190, 1311–1324. doi:10.1111/j.1365-246X.2012.05580.x.
- Karim, K.H., Koyi, H., Baziani, M.M., Hessami, K., 2011. Significance of angular unconformities between Cretaceous and Tertiary strata in the northwestern segment of the Zagros fold–thrust belt, Kurdistan. *Geol. Mag.* 148, 925–939. doi:10.1017/S0016756811000471.
- Keller, E.A., Gurolo, L., Tierney, T.E., 1999. Geomorphic criteria to determine direction of lateral propagation of reverse faulting and folding. *Geology* 27, 515–518.
- Koop, W.J., Stoneley, R., 1982. Subsidence history of the Middle East Zagros basin, Permian to recent. *Phil. Trans. Roy. Soc. Lond.: Mathematical, Physical and Engineering Sciences* 305, 149–168. doi:10.1098/rsta.1982.0031.
- Koshnaw, R.I., Horton, B.K., Stockli, D.F., Barber, D.E., TamarAgha, M.Y., Kendall, J.J., 2017. Neogene shortening and exhumation of the Zagros fold-thrust belt and foreland basin in the Kurdistan region of northern Iraq. *Tectonophysics* 694, 332–355. doi:10.1016/j.tecto.2016.11.016,2017.
- Koshnaw, R.I., Stockli, D.F., Schlunegger, F., 2018. Timing of the Arabia-Eurasia continental collision—evidence from detrital zircon U-Pb geochronology of the Red Bed Series strata of the northwest Zagros hinterland, Kurdistan region of Iraq. *Geology* 47, 47–50. doi:10.1130/G45499.1.
- Lacombe, O., Bellahsen, N., 2016. Thick-skinned tectonics and basement-involved fold–thrust belts: insights from selected Cenozoic orogens. *Geol. Mag.* 153, 763–810. doi:10.1017/S0016756816000078.
- Lavé, J., Avouac, J.P., 2001. Fluvial incision and tectonic uplift across the Himalayas of central Nepal. *Journal of Geophysical Research, Solid Earth* 106, 26,561–26,591. doi:10.1029/2001JB000359.
- Lawa, F.A., Koyi, H., Ibrahim, A., 2013. Tectono-stratigraphic evolution of the NW segment of the Zagros fold-thrust belt, Kurdistan, NE Iraq. *J. Petrol. Geol.* 36, 75–96. doi:10.1111/jpg.12543.
- Le Garzic, E., Vergés, J., Sapin, F., Saura, E., Meresse, F., Ringenbach, J.-C., 2019. Evolution of the NW Zagros Fold-and-Thrust Belt in Kurdistan Region of Iraq from balanced and restored crustal-scale sections and forward modelling. *J. Struct. Geol.* 124, 51–69. doi:10.1016/j.jsg.2019.04.006.
- Lescoutre, R., 2019. *Formation and Reactivation of the Pyrenean-Cantabrian Rift System: Inheritance, Segmentation and Thermal Evolution*. PhD thesis, Université Strasbourg.
- Mazzoli, S., Pierantoni, P.P., Borraccini, F., Paltrinieri, W., Deiana, G., 2005. Geometry, segmentation pattern and displacement variations along a major Apennine thrust zone, central Italy. *J. Struct. Geol.* 27, 1940–1953. doi:10.1016/j.jsg.2005.06.002.
- McQuarrie, N., 2004. Crustal scale geometry of the Zagros fold–thrust belt, Iran. *J. Struct. Geol.* 26, 519–535. doi:10.1016/j.jsg.2003.08.009.
- McQuarrie, N., van Hinsbergen, D.J., 2013. Retrodeforming the Arabia-Eurasia collision zone: age of collision versus magnitude of continental subduction. *Geology* 41, 315–318. doi:10.1130/G33591.1.
- Miller, S.R., Slingerland, R.L., 2006. Topographic advection on fault-bend folds: inheritance of valley positions and the formation of wind gaps. *Geology* 34, 769–772. doi:10.1130/G22658.1.
- Mohammed, S.A.G., 2006. Megaseismic section across the northeastern slope of the Arabian plate, Iraq. *GeoArabia* 11, 77–90.
- Molinaro, M., Leturmy, P., Guezou, J.-C., Frizon de Lamotte, D., Eshraghi, S.A., 2005. The structure and kinematics of the southeastern Zagros fold-thrust belt, Iran: from thin-skinned to thick-skinned tectonics. *Tectonics* 24, TC3007. doi:10.1029/2004TC001633.
- Mouthereau, F., Lacombe, O., Meyer, B., 2006. The Zagros folded belt (Fars, Iran): constraints from topography and critical wedge modelling. *Geophys. J. Int.* 165, 336–356. doi:10.1111/j.1365-246X.2006.02855.
- Mouthereau, F., Lacombe, O., Vergés, J., 2012. Building the Zagros collisional orogen: timing, strain distribution and the dynamics of Arabia/Eurasia plate convergence. *Tectonophysics* 532, 27–60. doi:10.1016/j.tecto.2012.01.022.
- Nissen, E., Tatar, M., Jackson, J.A., Allen, M.B., 2011. New views on earthquake faulting in the Zagros fold-and-thrust belt of Iran. *Geophys. J. Int.* 186 (3), 928–944. doi:10.1111/j.1365-246X.2011.05119.x.
- Obaid, A.K., Allen, M.B., 2017. Landscape maturity, fold growth sequence and structural style in the Kirkuk Embayment of the Zagros, northern Iraq. *Tectonophysics* 717, 27–40. doi:10.1016/j.tecto.2017.07.006.
- Oberlander, T.M., 1965. *The Zagros Streams: a New Interpretation of Transverse Drainage in an Orogenic Zone*. Syracuse University Press, p. 168.
- Paul, A., Hatzfeld, D., Kaviani, A., Tatar, A., Pequegnat, C., 2010. In: *Seismic Imaging of the Lithospheric Structure of the Zagros Mountain Belt (Iran)*, 330. Geological Society of London, Special Publication, pp. 5–18.
- Pérez-Peña, J.V., Al-Awabdeh, M., Azañón, J.M., Galve, J.P., Booth-Rea, G., Notti, D., 2017. Swath Profiler and NProfiler: two new ArcGIS Add-ins for the automatic extraction of swath and normalized river profiles. *Comput. Geosci.* 104, 135–150. doi:10.1016/j.cageo.2016.08.008.
- Pirouz, M., Simpson, G., Chiaradia, M., 2015. Constraint on foreland basin migration in the Zagros mountain belt using Sr isotope stratigraphy. *Basin Res.* 27, 714–728. doi:10.1111/bre.12097.
- Prince, P.S., Spotila, J.A., Henika, W.S., 2011. Stream capture as driver of transient landscape evolution in a tectonically quiescent setting. *Geology* 39, 823–826. doi:10.1130/G32008.1.
- Ramsey, L.A., Walker, R.T., Jackson, J., 2008. Fold evolution and drainage development in the Zagros mountains of Far province, SE Iran. *Basin Res.* 20, 23–48. doi:10.1111/j.1365-2117.2007.00342.x.
- Ranero, C.R., Morgan, J.P., McIntosh, K., Reichert, C., 2003. Bending-related faulting and mantle serpentinization at the Middle America trench. *Nature* 425, 367. doi:10.1038/nature01961.
- Ricou, L.E., Braud, J., Brunn, J.H., 1977. In: *Le Zagros*, 8. Mémoires de la Société Géologique de France, pp. 33–52.
- Saura, E., García-Castellanos, D., Casciello, E., Parravano, V., Urruela, A., Vergés, J., 2015. Modeling the flexural evolution of the Amiran and Mesopotamian foreland basins of NW Zagros (Iran-Iraq). *Tectonics* 34, 377–395. doi:10.1002/2014TC003660.
- Sepehr, M., Cosgrove, J.W., 2004. Structural framework of the Zagros fold–thrust belt, Iran. *Mar. Petrol. Geol.* 21, 829–843. doi:10.1016/j.marpetgeo.2003.07.006.
- Sherkati, S., Letouzey, J., 2004. Variation of structural style and basin evolution in the central Zagros (Izeh zone and Dezful Embayment), Iran. *Mar. Petrol. Geol.* 21 (5), 535–554. doi:10.1016/j.marpetgeo.2004.01.007.
- Sherkati, S., Letouzey, J., Frizon de Lamotte, D., 2006. Central Zagros fold-thrust belt (Iran): new insights from seismic data, field observation, and sandbox modelling. *Tectonics* 25, TC4007. doi:10.1029/2004TC001766.
- Snidero, M., Amilibia, A., Gratacos, O., Blanc, E.P., Muñoz, J.A., 2011. The 3D reconstruction of geological structures based on remote sensing data: example from the Anaran anticline, Lurestan province, Zagros fold and thrust belt, Iran. *J. Geol. Soc.* 168 (3), 769–782. doi:10.1144/0016-76492010-107.
- Stampfli, G.M., Borel, G.D., 2002. A plate tectonic model for the Paleozoic and Mesozoic constrained by dynamic plate boundaries and restored synthetic oceanic isochrons. *Earth Planet. Sci. Lett.* 196, 17–33. doi:10.1016/S0012-821X(01)00588-X.
- Stöcklin, J., 1968. Structural history and tectonics of Iran: a review. *AAPG (Am. Assoc. Pet. Geol.) Bull.* 52, 1229–1258.
- Sutra, E., Manatschal, G., Mohn, G., Unternehr, P., 2013. Quantification and restoration of extensional deformation along the Western Iberia and Newfoundland rifted margins. *G-cubed* 14, 2575–2597. doi:10.1002/ggge.20135.
- Szaniawski, R., Mazzoli, S., Jankowski, L., 2017. Controls of structural inheritance on orogenic curvature and foreland basin sedimentation: insights from the Przemysł area, Western Carpathians. *J. Struct. Geol.* 103, 137–150. doi:10.1016/j.jsg.2017.09.004.
- Talbot, C.J., Alavi, M., 1996. In: *The Past of a Future Syntaxis across the Zagros*, 100. Geological Society of London, Special Publication, pp. 89–109. doi:10.1144/GSL.SP.1996.100.01.08.
- Taleblian, M., Jackson, J.A., 2002. Offset on the main Recent Fault of the NW Iran and implications for the late Cenozoic tectonics of the Arabia-Eurasia collision zone. *Geophys. J. Int.* 150, 422–439. doi:10.1046/j.1365-246X.2002.01711.
- Taleblian, M., Jackson, J.A., 2004. A reappraisal of earthquake focal mechanisms and active shortening in the Zagros mountains of Iran. *Geophys. J. Int.* 156, 506–526. doi:10.1111/j.1365-246X.2004.02092.
- Tavani, S., Arbués, P., Snidero, M., Carrera García de Cortázar, N., Muñoz, J.A., 2011. Open Plot Project: an open-source toolkit for 3-D structural data analysis. *Solid Earth* 2, 53–63. doi:10.5194/se-2-53-2011.
- Tavani, S., Carola, E., Granado, P., Quintá, A., Muñoz, J.A., 2013. Transpressive inversion of a Mesozoic extensional forced fold system with an intermediate décollement level in the Basque-Cantabrian Basin (Spain). *Tectonics* 32, 146–158. doi:10.1002/tect.20019.
- Tavani, S., Storti, F., Lacombe, O., Corradetti, A., Muñoz, J.A., Mazzoli, S., 2015. A review of deformation pattern templates in foreland basin systems and fold-and-thrust belts: implications for the state of stress in the frontal regions of thrust wedges. *Earth Sci. Rev.* 141, 82–104. doi:10.1016/j.earscirev.2014.11.013.
- Tavani, S., Parente, M., Puzone, F., Corradetti, A., Gharabegli, G., Valinejad, M., Morsalnejad, D., Mazzoli, S., 2018. The seismogenic fault system of the 2017 Mw 7.3 Iran-Iraq earthquake: constraints from surface and subsurface data, cross-section balancing and restoration. *Solid Earth* 9, 821–831. doi:10.5194/se-9-821-2018.
- Tavani, S., Parente, M., Vitale, S., Iannace, A., Corradetti, A., Bottini, C., Morsalnejad, D., Mazzoli, S., 2018. Early Jurassic rifting of the Arabian passive continental margin of the Neo-Tethys. Field evidence from the Lurestan region of the Zagros fold-and-thrust belt, Iran. *Tectonics* 27, 2586–2607. doi:10.1029/2018TC005192.
- Tavani, S., Corradetti, A., Sabbatino, M., Morsalnejad, D., Mazzoli, S., 2018. The Meso-Cenozoic fracture pattern of the Lurestan region, Iran: the role of rifting, convergence, and differential compaction in the development of preorogenic oblique fractures in the Zagros Belt. *Tectonophysics* 749, 104–119. doi:10.1016/j.tecto.2018.10.031.
- Tugend, J., Manatschal, G., Kusznir, N.J., Masini, E., Mohn, G., Thoin, I., 2014. Formation and deformation of hyperextended rift systems: insights from rift domain map

- ping in the Bay of Biscay-Pyrenees. *Tectonics* 33, 1239–1276. doi:10.1002/2014TC003529.
- Vajedian, S., Motagh, M., Mousavi, Z., Motaghi, K., Fielding, E., Akbari, B., Wetzel, H.H., Darabi, A., 2018. Coseismic deformation field of the MW 7.3 12 November 2017 Sarpol-e Zahab (Iran) earthquake: a decoupling horizon in the northern Zagros Mountains inferred from InSAR observations. *Rem. Sens.* 10, 1589. doi:10.3390/rs10101589.
- Vergés, J., Saura, E., Casciello, E., Fernández, M., Villaseñor, A., Jiménez-Munt, I., García-Castellanos, D., 2011. Crustal-scale cross-sections across the NW Zagros belt: implications for the Arabian margin reconstruction. *Geol. Mag.* 148, 739–761. doi:10.1017/S0016756811000331.
- Vergés, J., Goodarzi, M.G.H., Emami, H., Karpuz, R., Efstathiou, J., Gillespie, P., 2011. Multiple detachment folding in Pusht-e Kuh arc, Zagros: role of mechanical stratigraphy. In: McClay, K., Shaw, J., Suppe, J. (Eds.), *Thrust Fault Related Folding*, 94. AAPG Memoir, pp. 69–94. doi:10.1306/13251333M942899.
- Vernant, P., Nilforoushan, F., Hatzfeld, D., Abbassi, M.R., Vigny, C., Masson, F., Nankali, H., Martinod, J., Ashtiani, A., Bayer, R., Tavakoli, F., Chéry, J., 2004. Present-day crustal deformation and plate kinematics in the Middle East constrained by GPS measurements in Iran and northern Oman. *Geophys. J. Int.* 157, 381–398. doi:10.1111/gji.2004.157.
- Walker, R.T., Ramsey, L.A., Jackson, J., 2011. Geomorphic evidence for ancestral drainage pattern in the Zagros Simple Folded Zone and growth of the Iranian plateau. *Geol. Mag.* 148, 901–910. doi:10.1017/S0016756811000185.
- Wells, D.L., Coppersmith, K.J., 1994. New empirical relationships among magnitude, rupture length, rupture width, rupture area, and surface displacement. *Bull. Seismol. Soc. Am.* 84, 974–1002.
- Williams, G.D., Powell, M.A., Cooper, M.A., 1989. In: *Geometry and Kinematics of Inversion Tectonics*, 44. Geological Society of London, Special Publications, pp. 3–15. doi:10.1144/GSL.SP.1989.044.01.02.
- Wrobel-Daveau, J.-C., Ringenbach, J.-C., Tavakoli, S., Ruiz, G.M.H., Masse, P., Frizon de Lamotte, D., 2010. Evidence for mantle exhumation along the Arabian margin in the Zagros (Kermanshah area, Iran). *Arabian Journal of Geosciences* 3, 499–513. doi:10.1007/s12517-010-0209-z.
- Zebari, M., Grützner, C., Navabpour, P., Ustaszewski, K., 2019. Relative timing of uplift along the Zagros mountain front flexure (Kurdistan region of Iraq): constrained by geomorphic indices and landscape evolution modeling. *Solid Earth* 663–682. doi:10.5194/se-10-663-2019.
- Ziegler, M.A., 2001. Late Permian to Holocene paleofacies evolution of the Arabian plate and its hydrocarbon occurrences. *GeoArabia* 6, 445–504.